An overall summary of my activities as a doctoral student

Patrick Asenov

Institute of Nuclear and Particle Physics
NCSR "Demokritos"

October 9, 2020

H.F.R.I.
Hellenic Foundation for Research & Innovation

Outline

- The HL-LHC and CMS Phase-2 upgrades
- Silicon sensors
- High-rate particle telescopes

The Large Hadron Collider (LHC)

- The world's largest and highest-energy particle accelerator
- The largest machine in the world
- A 27 km ring of superconducting magnets
- Accelerates protons, lead ions
- Two beams traveling in opposite directions $\rightarrow$ collisions
- Record energy of 13 TeV (6.5 TeV per beam) for protons; frequency: 40 MHz
- 4 large experiments: ALICE, ATLAS, CMS, LHCb

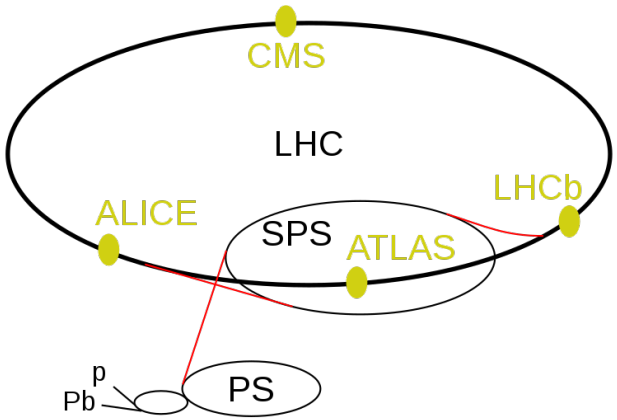

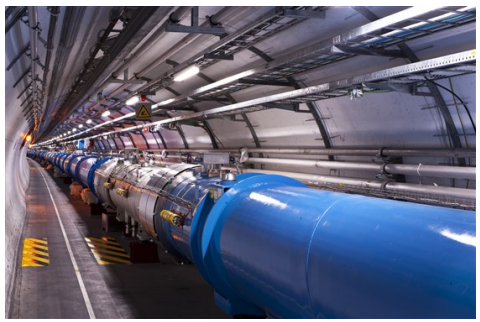

The physics goals of the LHC

- 4 July 2012, CMS and ATLAS: Higgs boson ($\sim$ 125 GeV)
- 8 October 2013, Nobel prize in physics: F. Englert and P. Higgs
- Questions unanswered:
  - nature of dark matter
  - nature of datk energy
  - what happened to the antimatter after BB
  - different mass scale of quark/lepton generations
  - mechanism through which neutrinos obtain their mass
  - extra dimensions
  - nature and properties of quark-gluon plasma

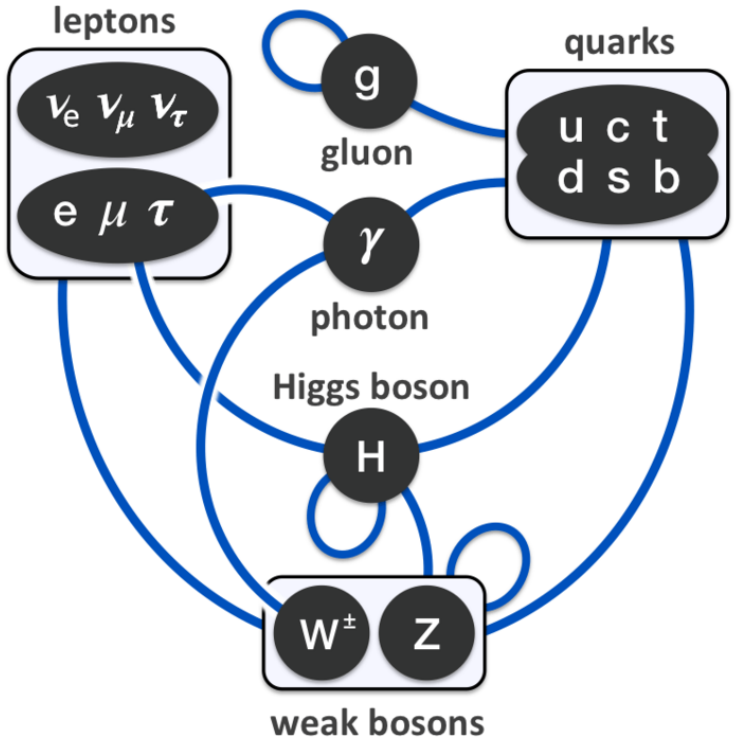

The High-Luminosity Upgrade

Objective: to increase the luminosity of LHC by a factor of 10 beyond its initial design value (peak luminosity: 5×10^{34} cm^{-2}s^{-1}, total expected integrated luminosity: 3000 fb^{-1})

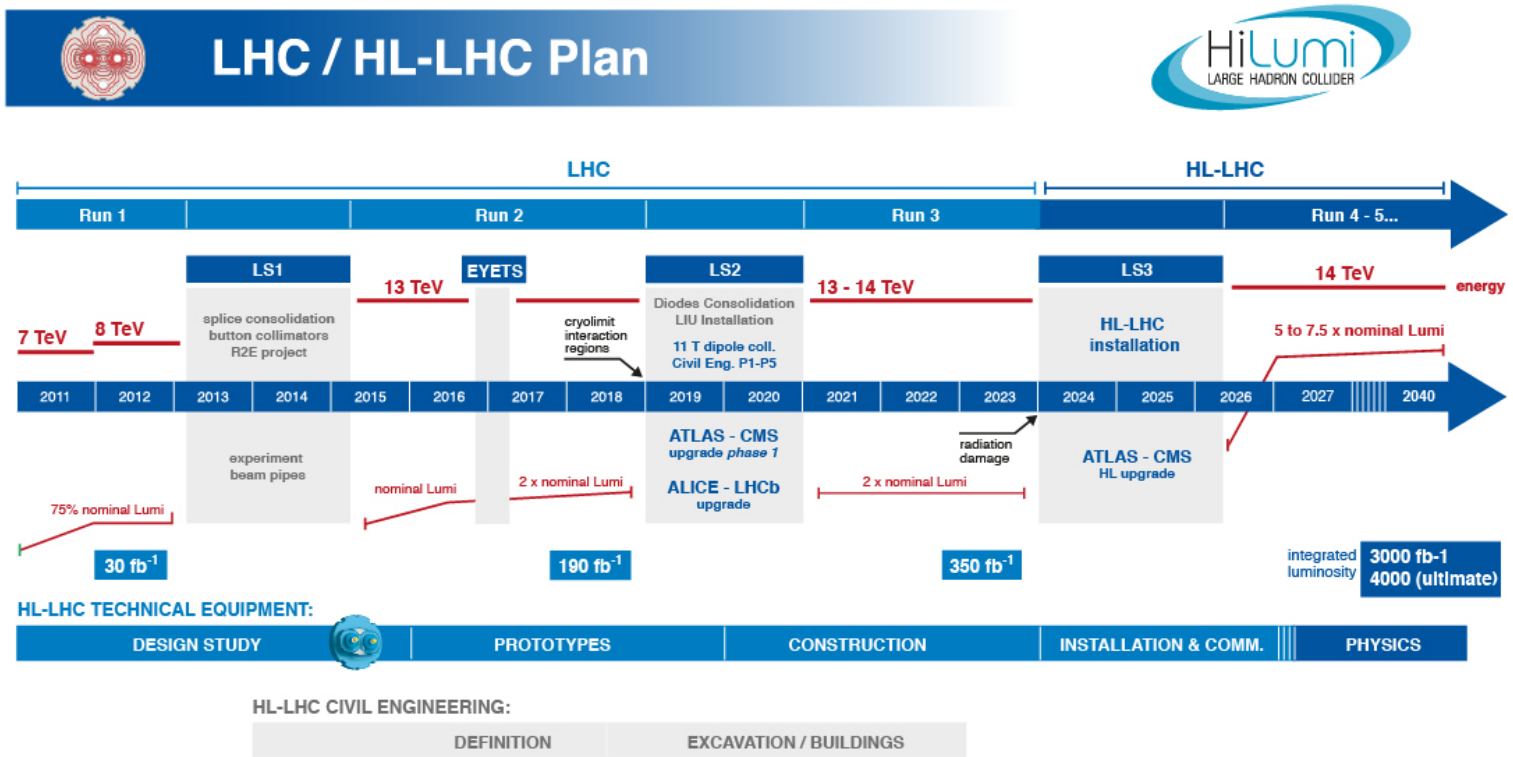

Novel technologies for the HL-LHC

- Cutting-edge 11-12 T superconducting magnets
- Compact superconducting crab cavities with ultra-precise phase control for beam rotation
- New technology for beam collimation
- High-power superconducting links with almost zero energy dissipation

The CMS detector

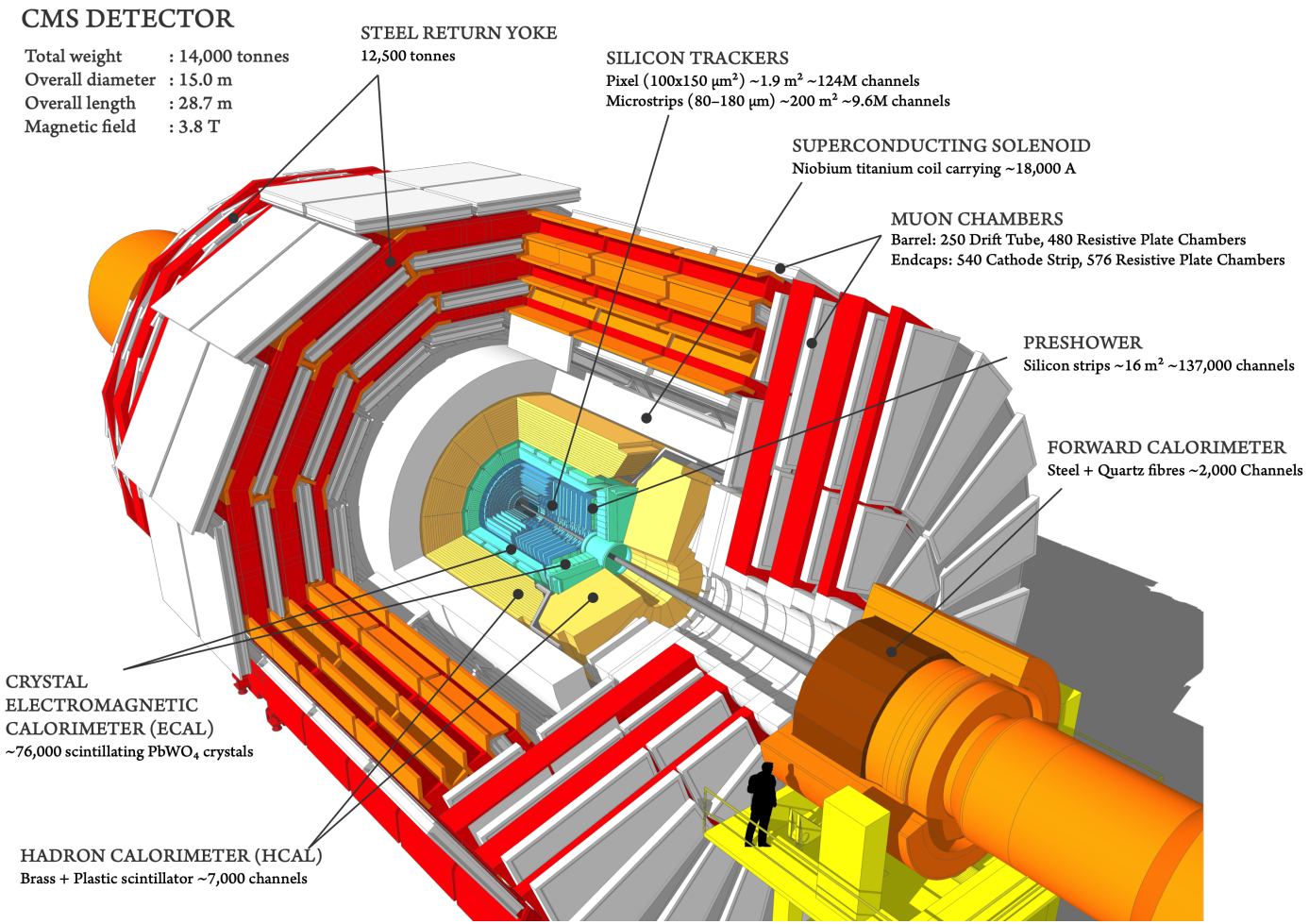

Specific particle interactions in the CMS detector

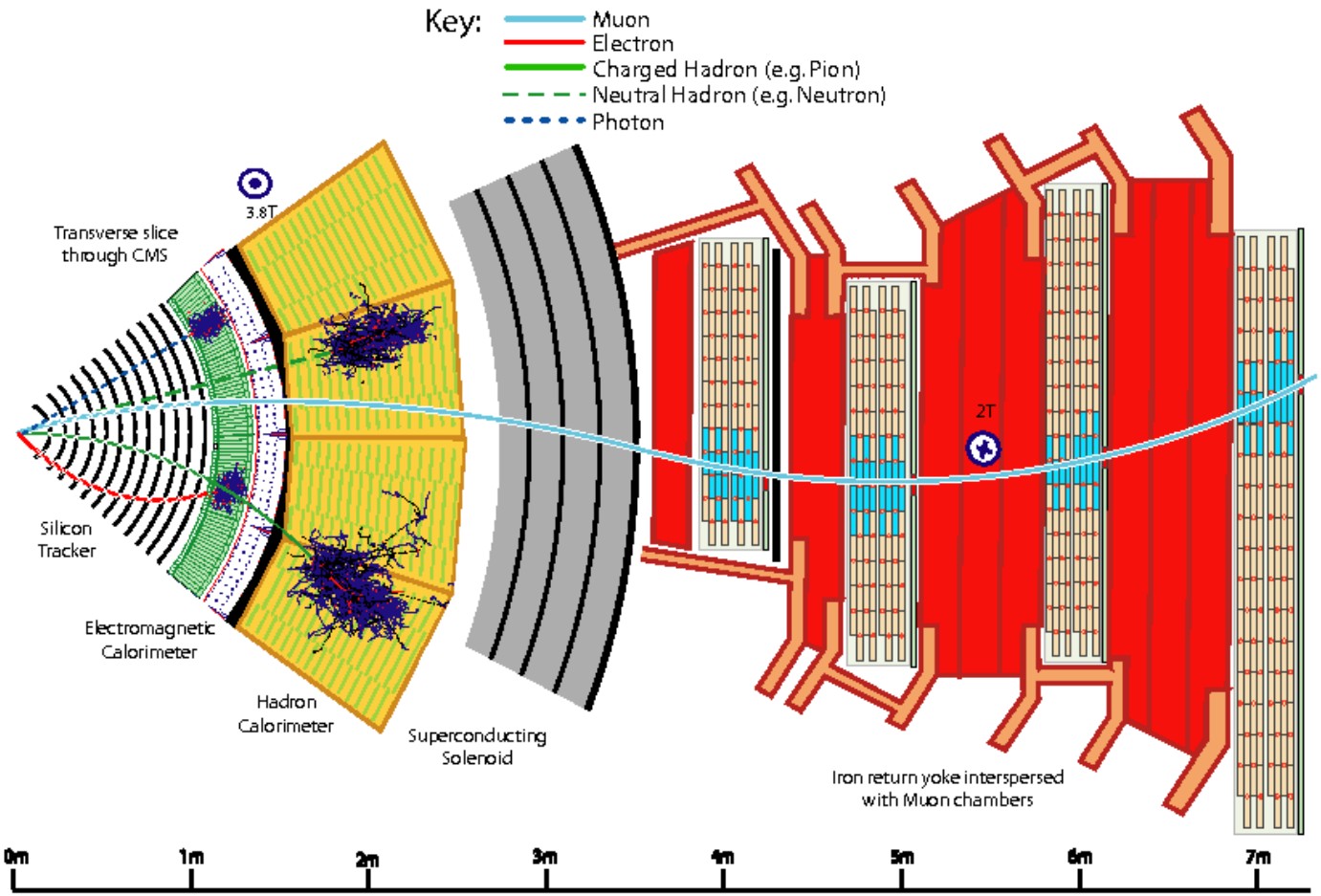

The Phase-2 Upgrade of the CMS Tracker

- Inner Tracker
  - unprecedented radiation levels of 1.2 Grad and $2.3 \times 10^{16}\,\mathrm{n_{eq}/cm^2}$ and hit rate of 3.2 GHz/cm^2
  - hybrid pixel modules: pixel sensors (pixel size of 2500 μm^2) and a new 65 nm CMOS ASIC (RD53)
  - novel scheme of serial powering
  - high bandwidth readout system
  - lightweight mechanics based on carbon-fibre material
  - two-phase CO_2 cooling
- Outer Tracker
  - increased radiation hardness, higher granularity and track separation, compatibility with higher data rates and a longer trigger latency
  - modules with two closely spaced sensors read out by a single ASIC which will correlate data from both sensors to form short track segments (stubs), to be used in tracking at Level-1 trigger

Tracker layout

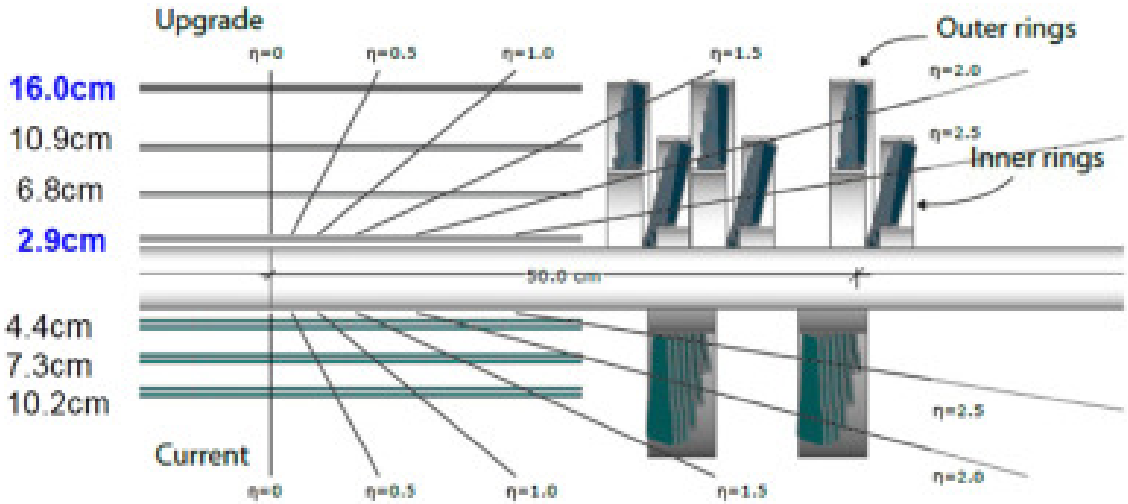

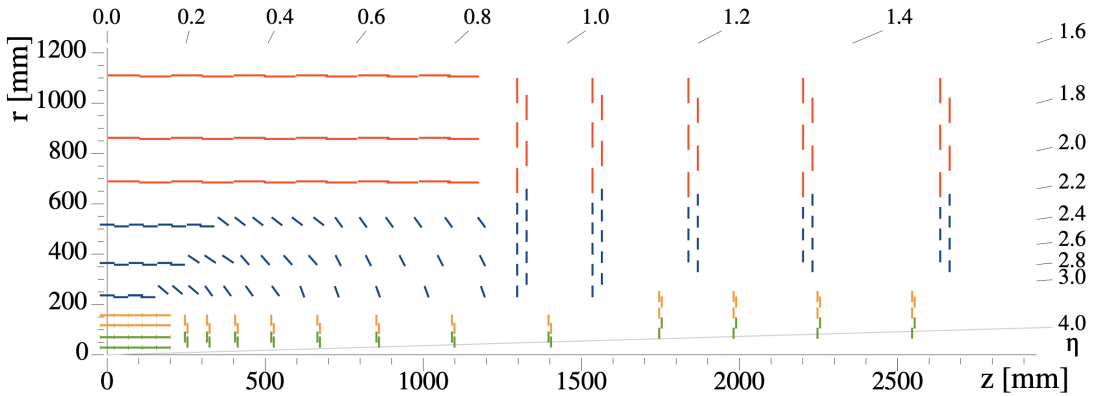

The p_T module concept

- The basic unit of the OT is a p_T module
  - Endcap Disks and Barrel region: 2S (outer regions, above R≈60 cm) and PS modules (radial range between R≈20 cm and R≈60 cm)
  - two closely spaced silicon sensors (2S: two sensors with micro-strips; PS one sensor with micro-strips and one sensor with macro-pixels)
  - read out by common front-end ASICs: correlating the hits from the two sensors
  - reject signals with p_T smaller than a given threshold

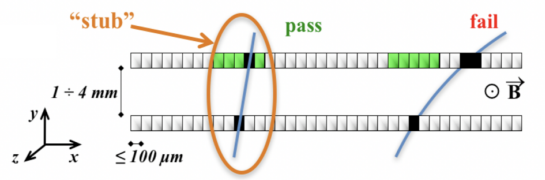

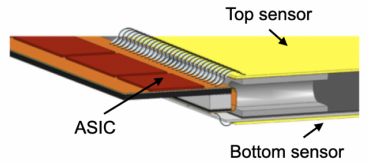

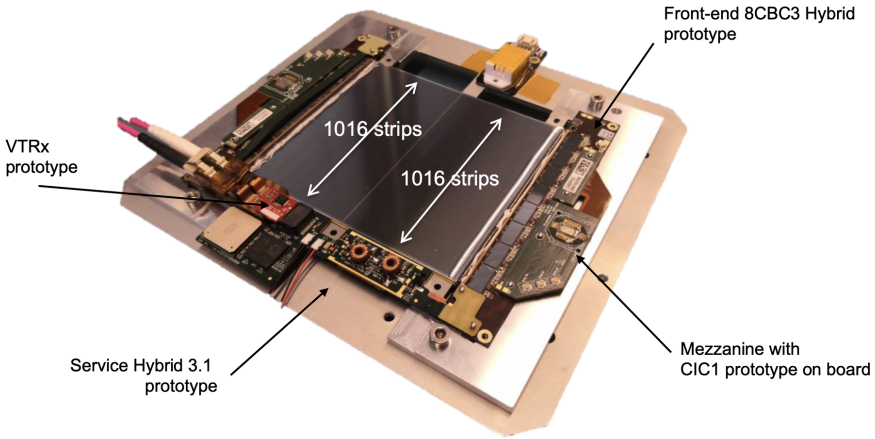

Stubs in the p_T module

Front-end ASIC: 1. receives the locations of hits in the transverse plane by a p_T-dependent angle, 2. measures the local distance, 3. compares it to a predefined acceptance window to select candidates with high p_T. A track stub (a type of a local track segment and matching pair of hits in the two sensors of a module within a given acceptance window) is formed and subsequently pushed out to the L1 trigger system at every bunch crossing.

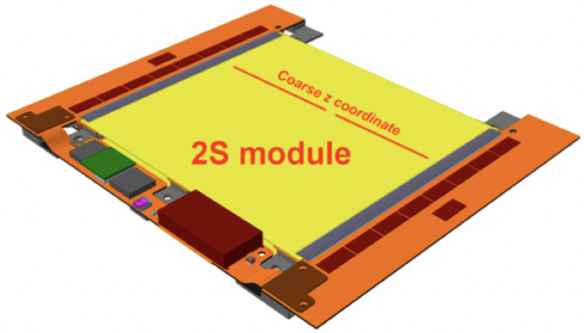

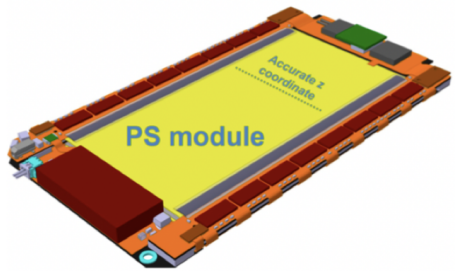

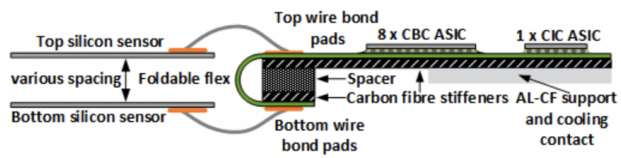

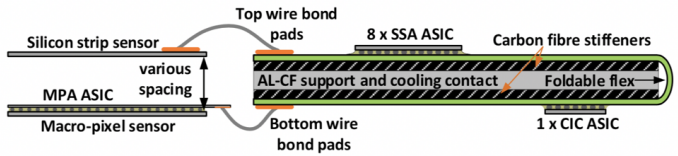

Principles of semiconductor devices

Images taken from: Zeghbroeck, Principles of Semiconductor Devices and Heterojunctions, Prentice Hall; F. Hartmann, Evolution of Silicon Sensor Technology in Particle Physics, Springer Tracts Mod.Phys. 275 (2017)

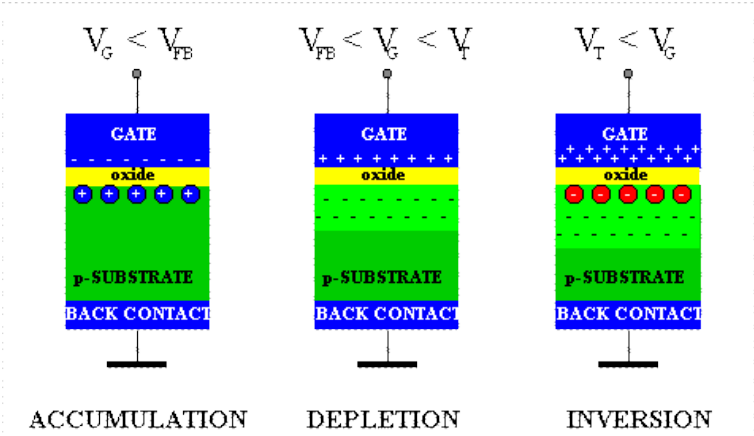

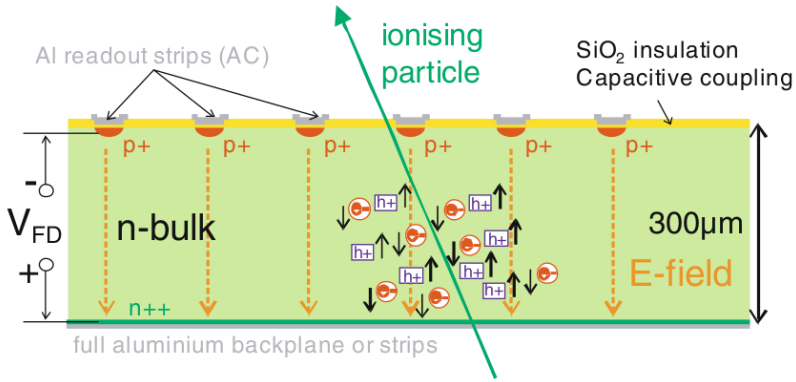

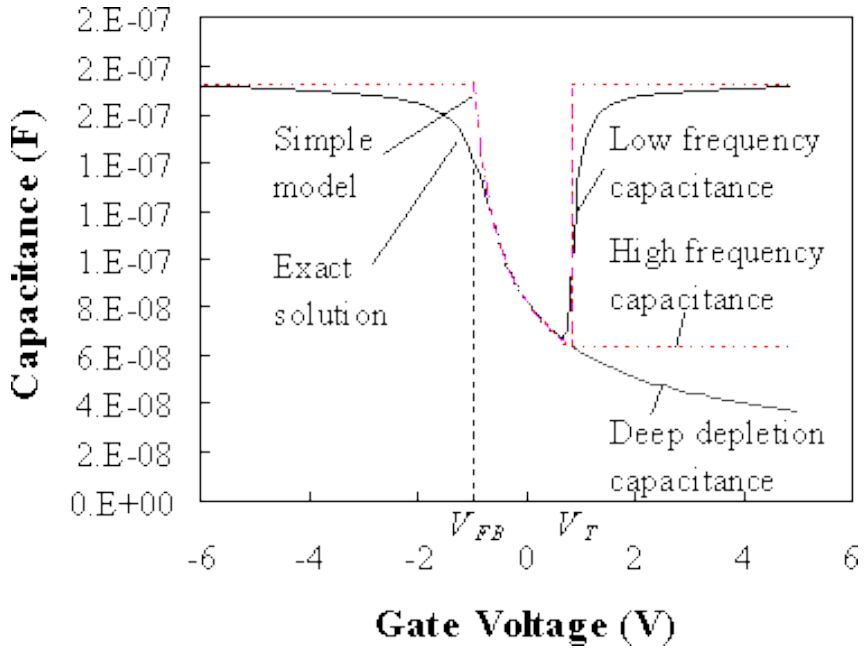

Particle-matter interaction

Images taken from: M. Tanabashi et al., Review of Particle Physics, Phys. Rev. D 98, 030001

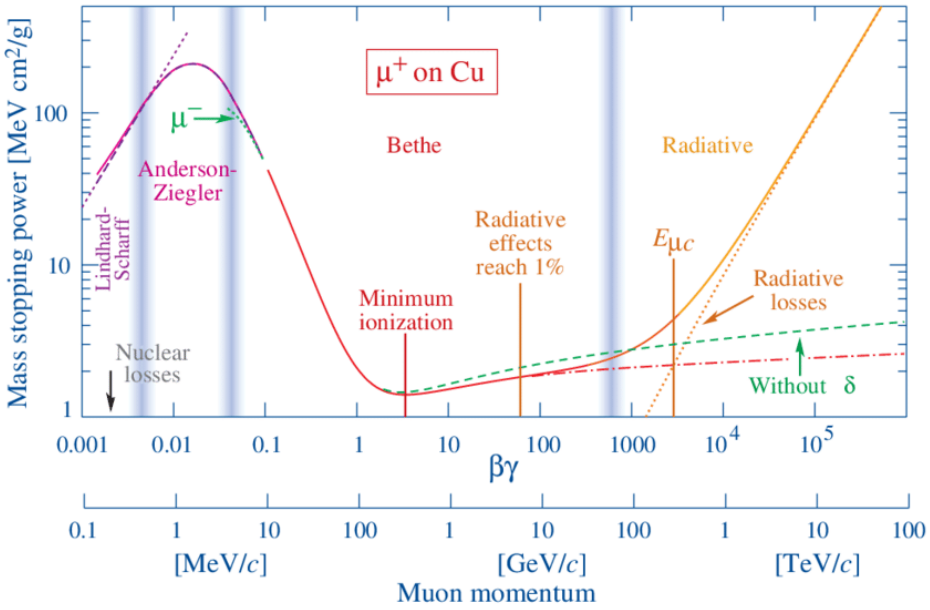

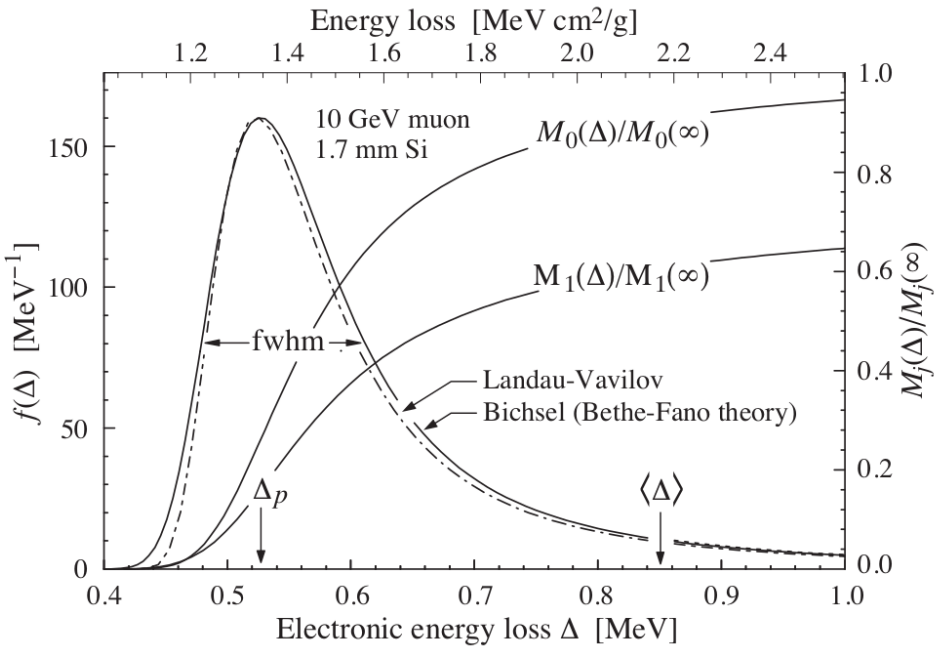

Hamamatsu Photonics K.K. wafers with 2S sensors and test structures

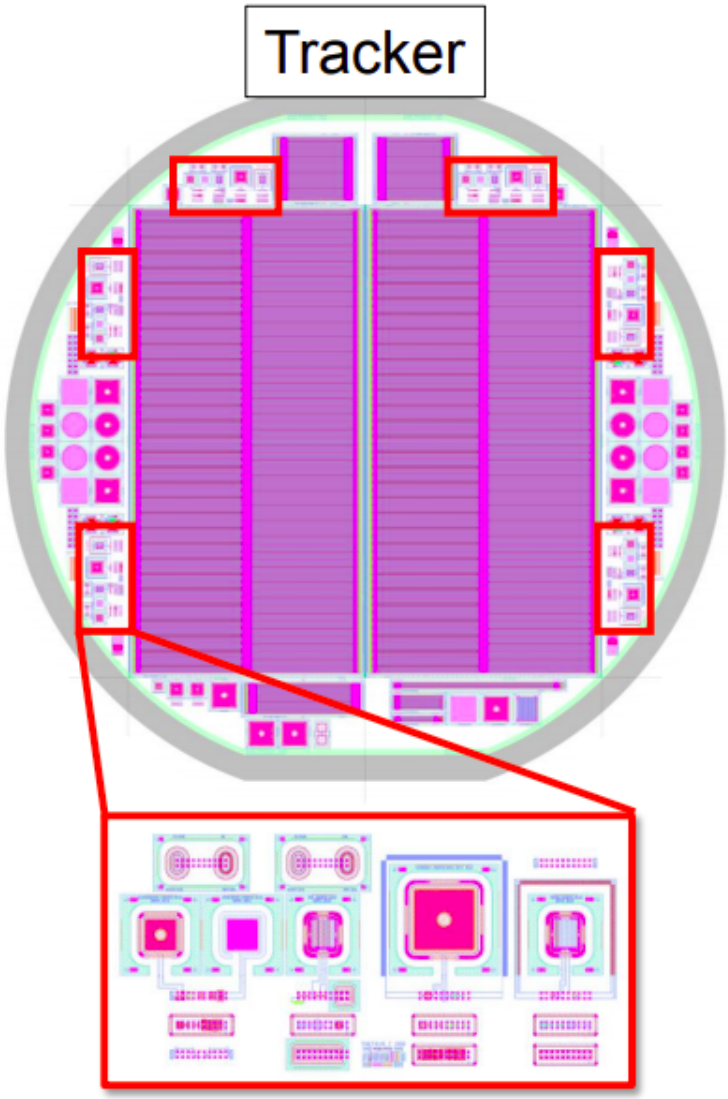

The Tracker quality control process

Vendor Quality Control (VQC), Sensor Quality Control (SQC), Process Quality Control (PQC), Irradiation Tests (IT)

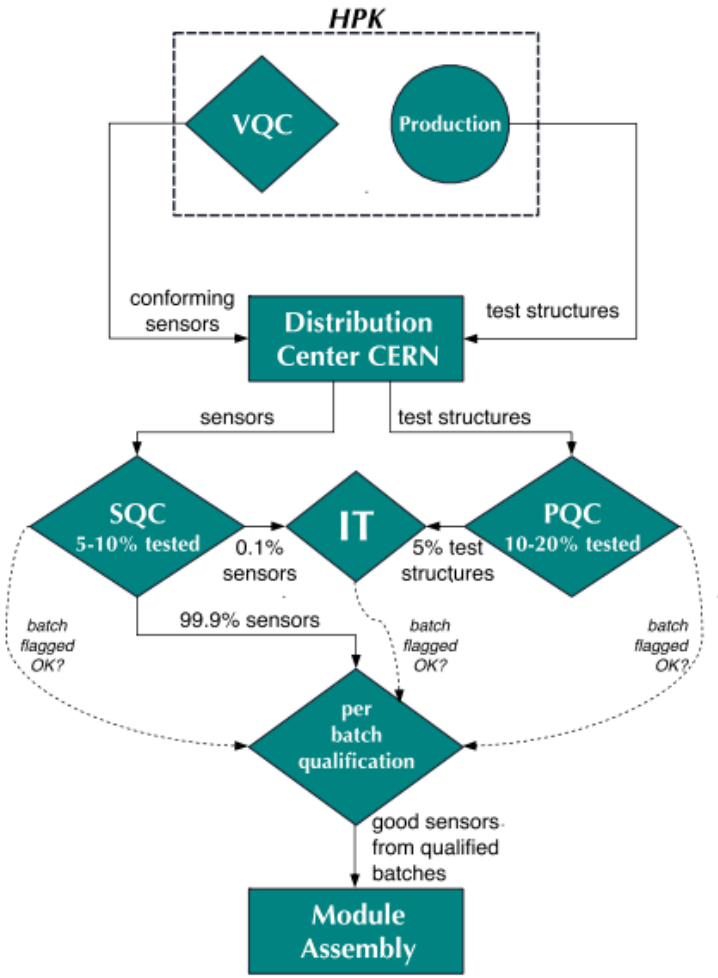

Structures set for automated PQC are located on wafers containing sensors for 2S modules (images from PQC spec. doc.)

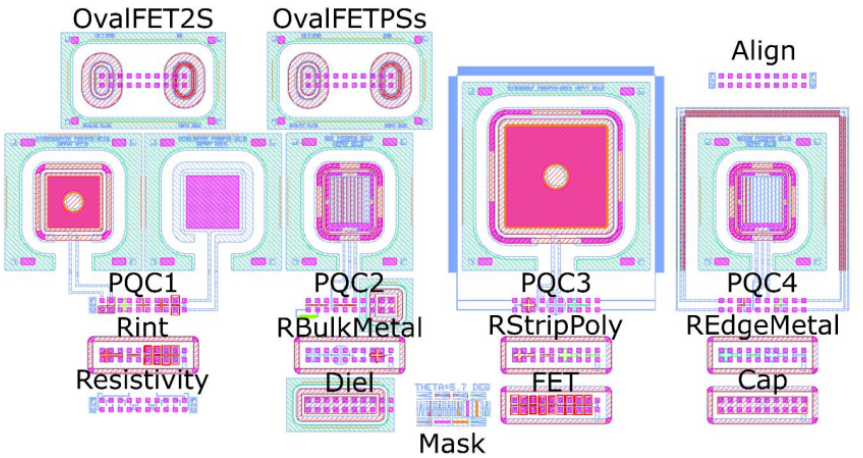

The Detector Instrumentation Laboratory (DIL) at NCSR "Demokritos"

- Area of 120 m^2 under temperature and humidity control
- Meaco 20L Low Energy Dehumidifier
- High dry air quality through an Atlas Copco oil-free air compressor
- Electrical characterization performed using a Carl Suss PA 150 automatic probe station and supplementary equipment (impedance analyzer for CV measurements, electrometer/high resistance meter and SourceMeter for IV measurements, switching matrix and Matrix Card for switching between IV and CV measurements)
- Operation through LabVIEW virtual instruments (VIs)
- Environmental simulations with regard to extreme temperature and humidity performed with a climate test chamber Weiss WKS 3-180/40/5

The automatic probe station at DIL

5 mm sized (full) diodes: IV measurements

2S sensor: $\sim$ 10 cm $\times$ 10 cm
(Active area of a 2S sensor)/(Active area of a full diode) $\approx$ 400
Left: Measurements of diodes at NCSR "Demokritos"
Right: Measurements of sensors at UoR

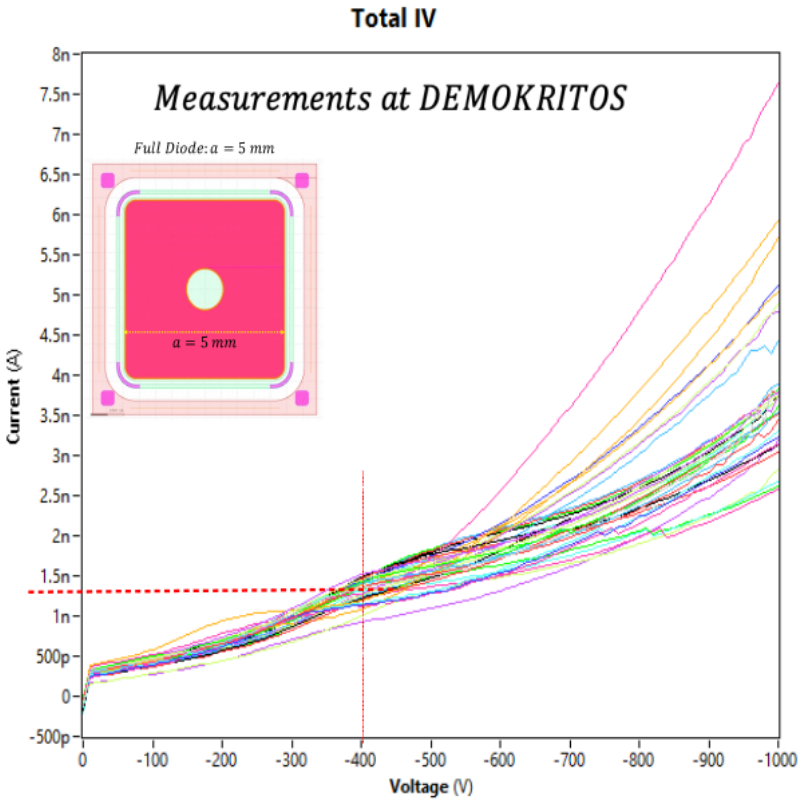

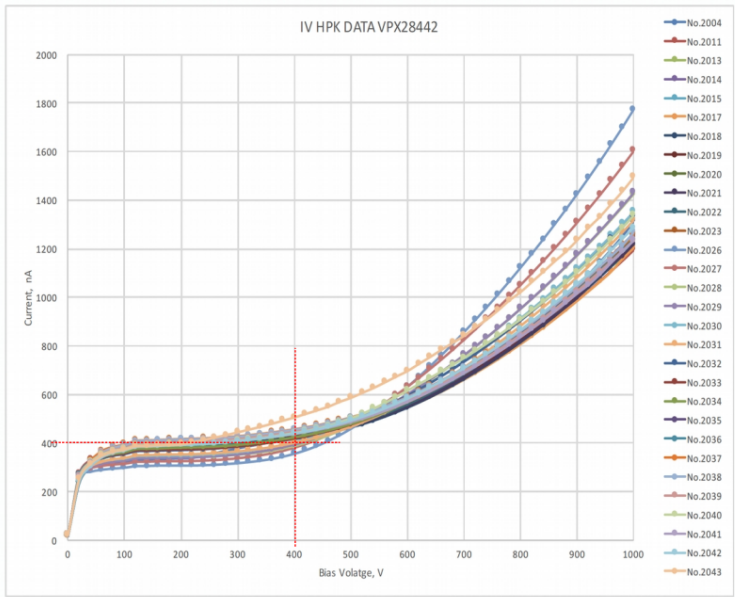

MOS capacitors: CV measurements

MOS capacitor: $|V_{FB}|$ must be smaller than 5 V
$|V_{FB}|$ can be evaluated from the CV curve of the MOS capacitor using its inflection point (a point on a continuous plane curve at which the curve changes from being concave to convex, or vice versa $\rightarrow$ where the second derivative is 0)

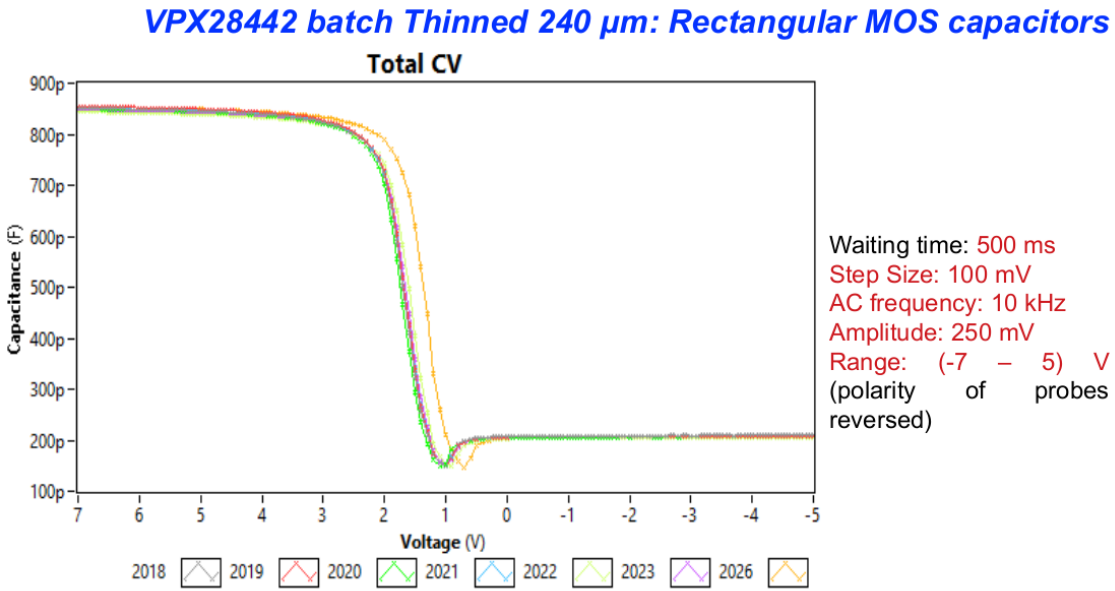

1.25 mm sized (quarter) diode: climate tests

$V = -350\,\mathrm{V}$, room temperature, different values of RH

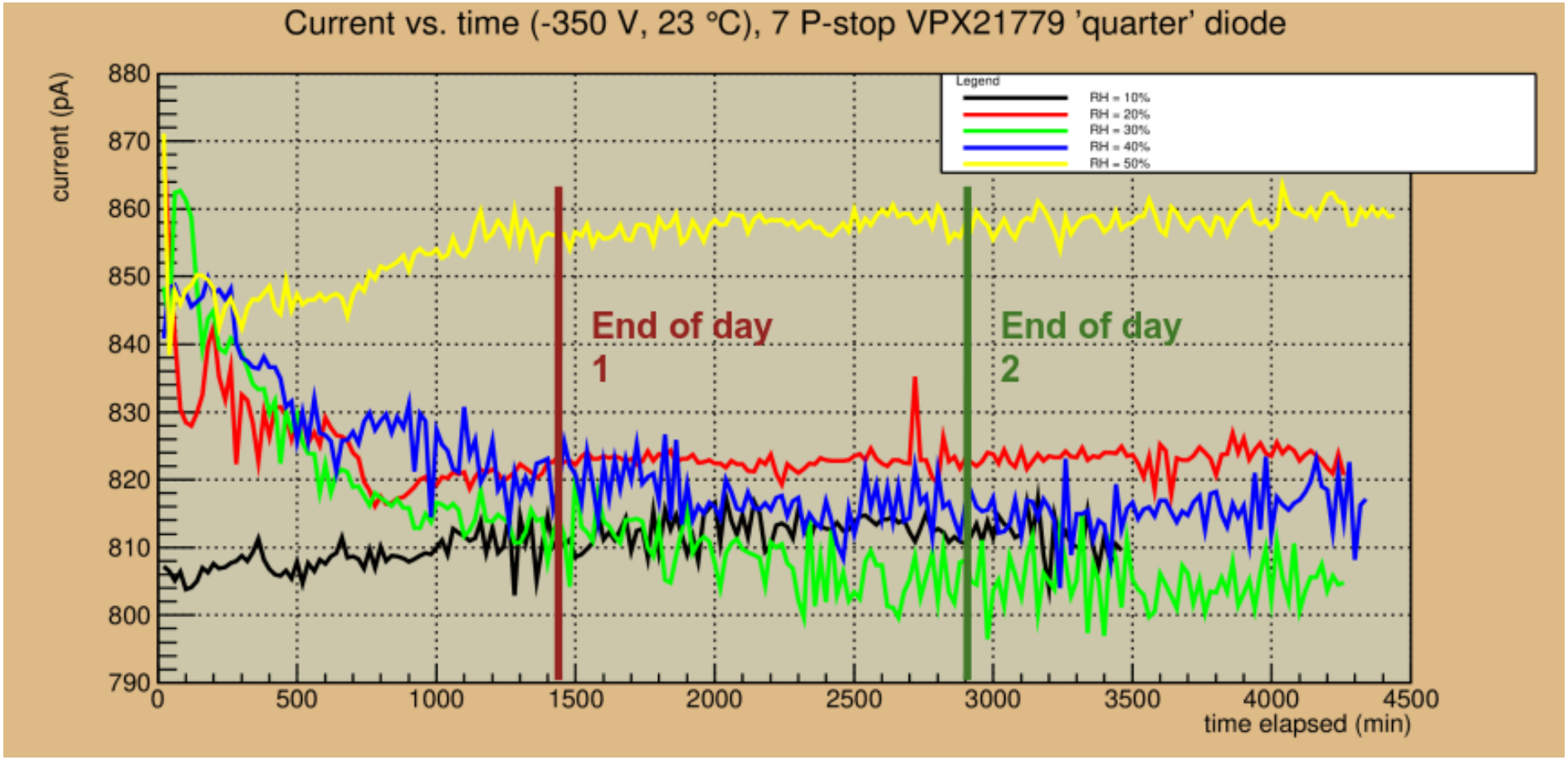

Irradiation campaign with a ^{60}Co source

HPK float-zone oxygenated silicon n-in-p test structures (thinned at 240 μm), containing MOS capacitors and diodes, were irradiated at the secondary standard ionizing radiation laboratory of the Greek Atomic Energy Commission (GAEC)

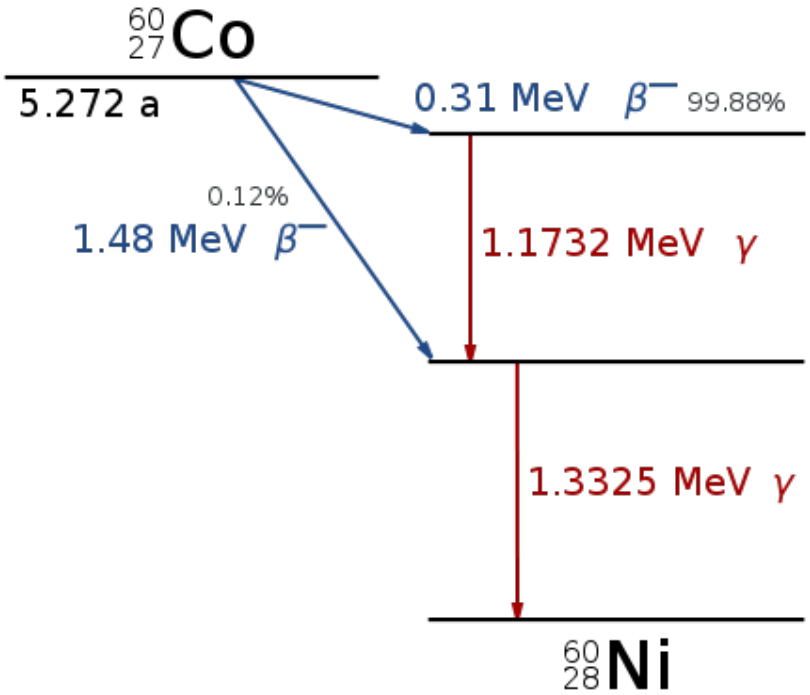

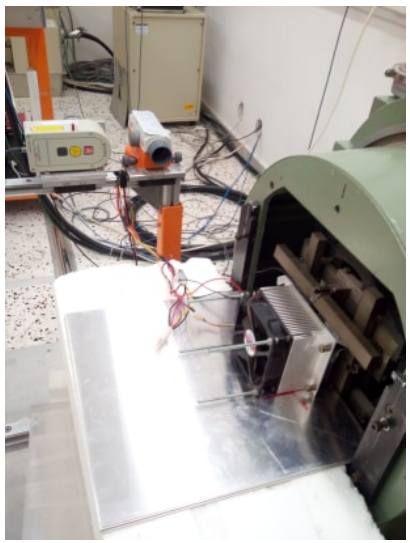

Equipment for the irradiation campaign

Charged particle equilibrium (CPE) $\rightarrow$ box of 2 mm-thick Pb and 0.8 mm of inner lining Al sheet $\rightarrow$ for the absorption of low energy photons and secondary electrons (ESCC Basic Specification No. 22900)

- Calculated dose rate (in air) at irradiation point (40 cm from the source): 0.96 kGy/h using FC65-P Ionization Chambers from IBA Dosymetry
- Peltier element/thermoelectric cooler with glue protection to withstand radiation, fan, microcontroller for stabilization of temperature, power supplies

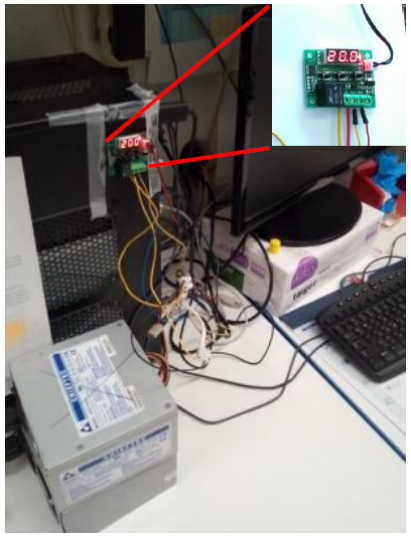

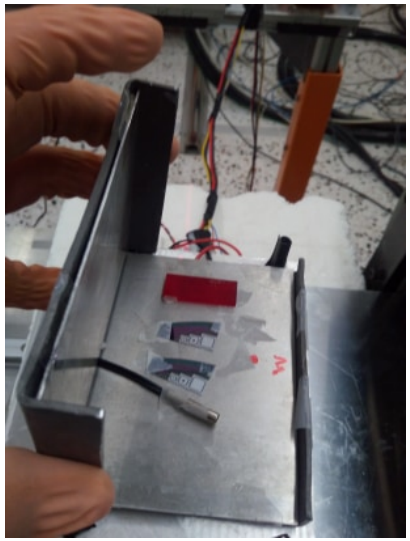

^{60}Co energy spectrum

Taken 4 m away from the cobalt-60 source and after 5.2 cm of Pb (a 5 cm thick Pb block was placed between the source and the CPE box and the Pb thickness of the CPE box was 0.2 cm), as measured inside the charged particle equilibrium (CPE) box

Left peak: a backscatter peak at approximately 200 keV which emerges when γ-rays enter the material around the detector and are scattered back into the detector

Right peaks: corresponding to the gamma-ray decay modes.

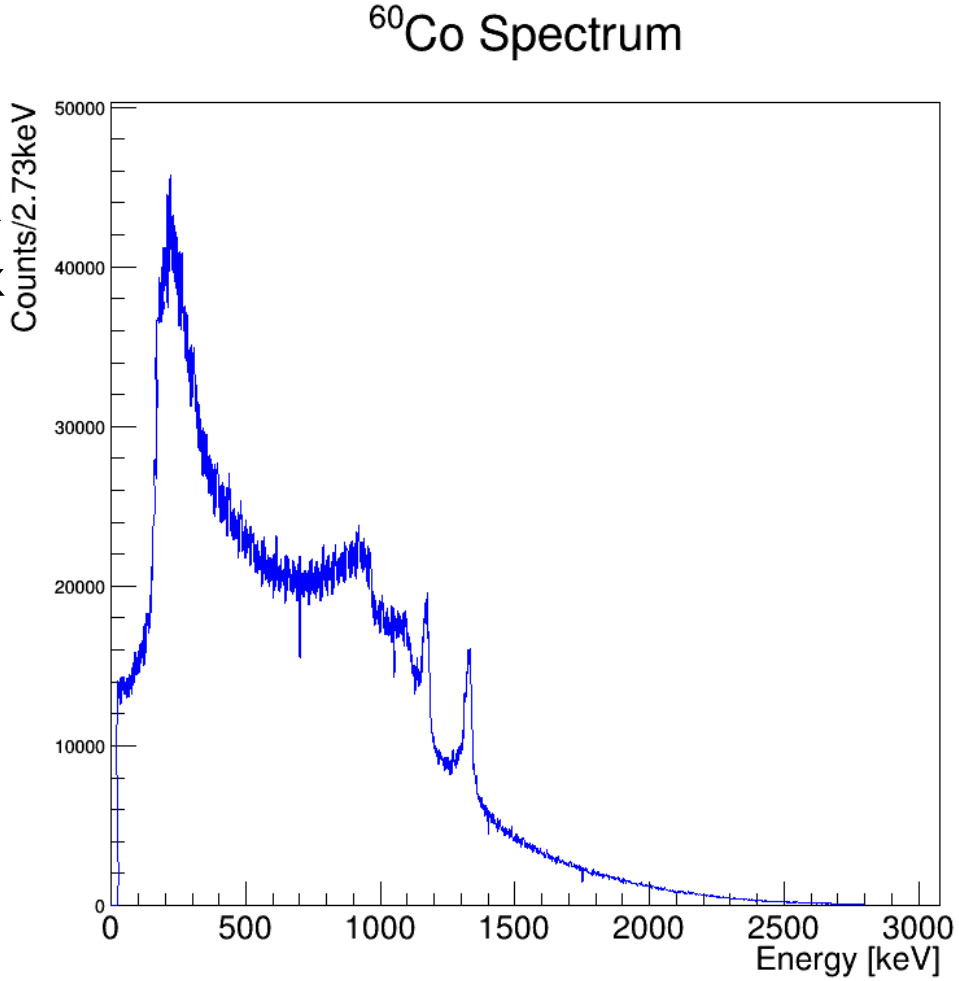

Irradiation protocol

- Irradiation procedure was split in slots of 6-16 hours of irradiation
- During irradiation temperature kept below 20.0 °C
- After every irradiation slot:
  - annealing in the climate test chamber at 60 °C for 10 min (corresponding to 4 days of annealing at room temperature)
  - electrical tests after annealing performed using our experimental setup
  - electrical measurements: 1) Oscillation level = 250 mV; 2) Various frequencies: 100 Hz, 1 kHz, 10 kHz, 100 kHz, 1 MHz
- Between irradiation slots: samples stored in freezer at -28 °C

MOS capacitor: CV measurements

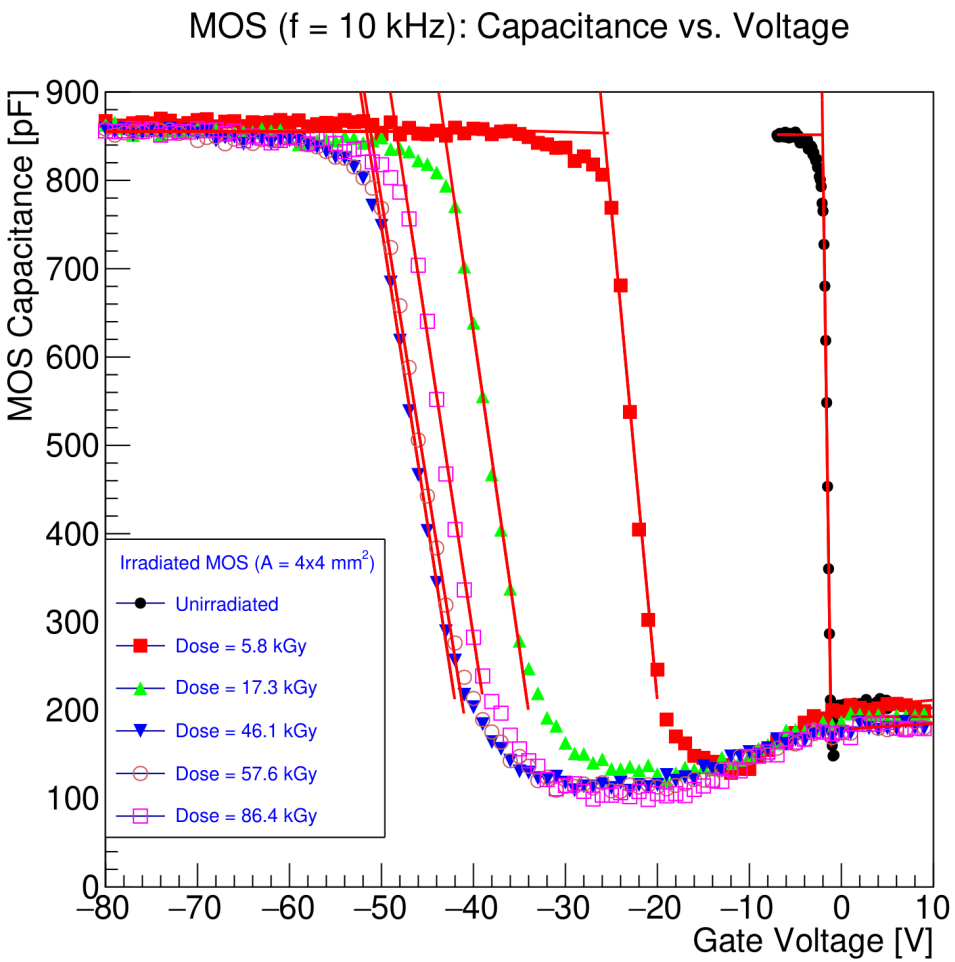

- Clear evidence of positive charge induced in the oxide of the MOS structures after exposure to γ-photons
- Initial shift of the flat band voltage (V_{FB}), i.e. the voltage where the MOS behavior changes from accumulation to depletion, to higher absolute values

MOS features from CV (1)

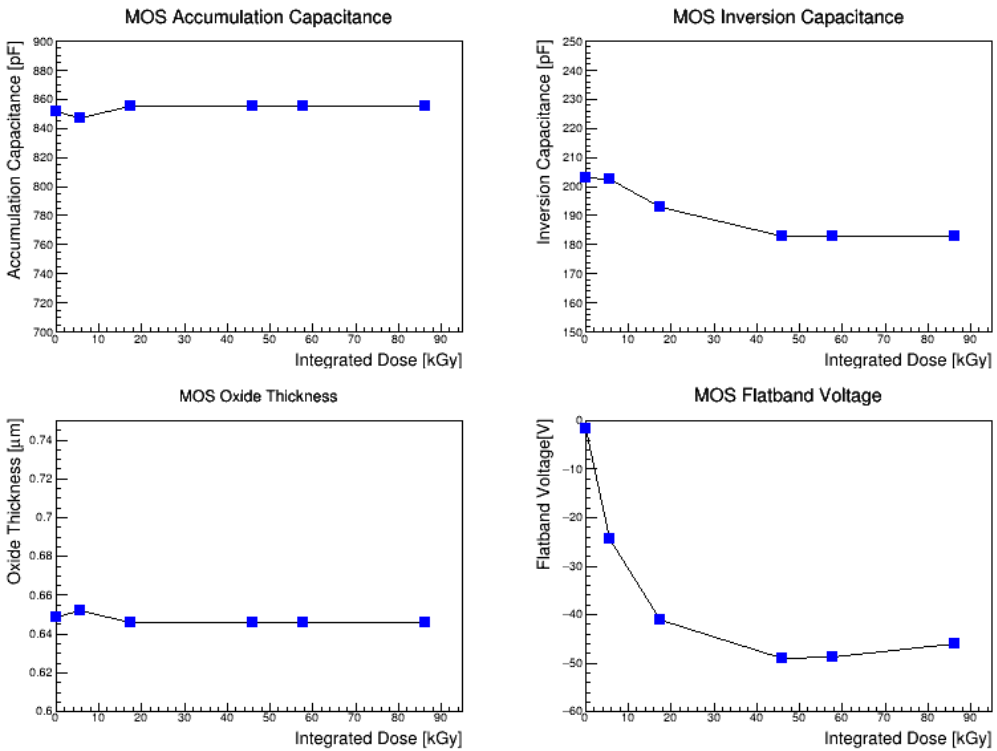

- MOS accumulation capacitance variation $<$ 4%
- MOS inversion capacitance variation $<$ 10%

Oxide thickness not affected because it is a geometric characteristic of the device ($t_{ox} = \frac{\epsilon_{ox}}{C_{ox}}$), $C_{ox} \rightarrow$ from accumulation region

MOS features from CV (2)

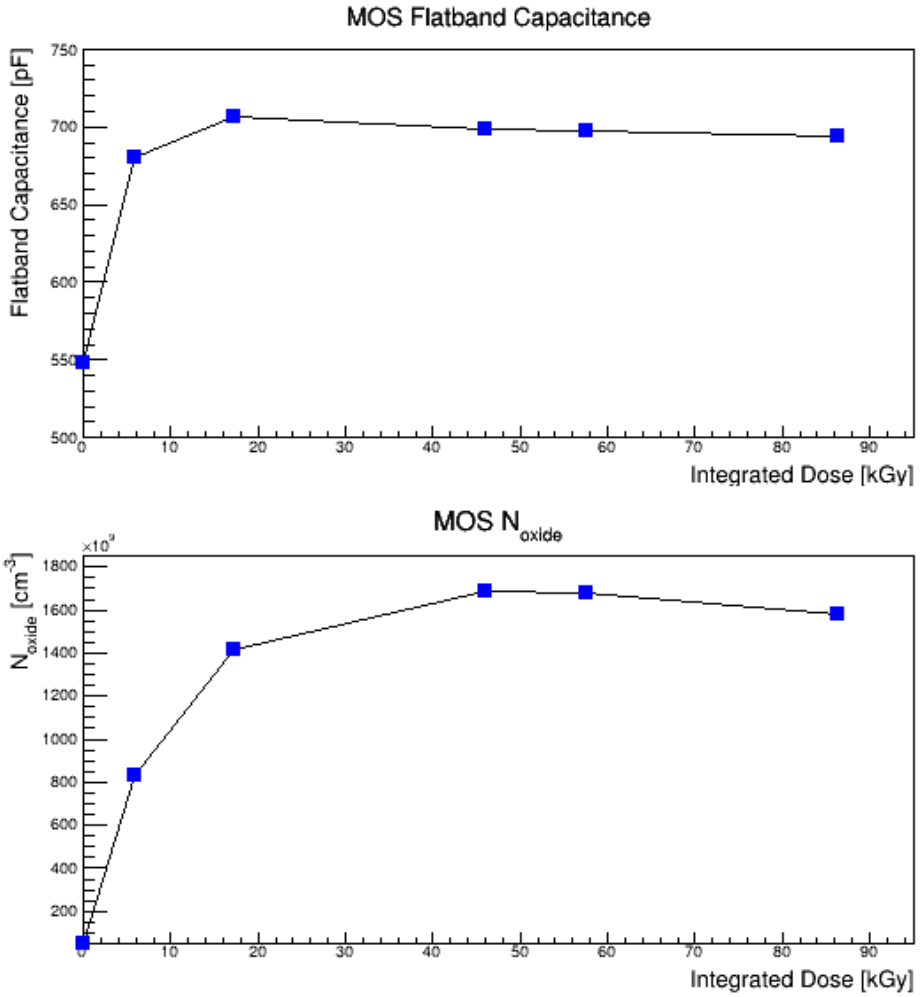

Flatband capacitance increases after initial irradiation but remains almost stable afterwards

$$C_{FB} = \frac{1}{\frac{1}{C_{ox}} + \frac{L_D}{\epsilon_s}}$$

where L_D is the Debye length

2.5 mm sized (half) diode: IV measurements

Scaling to 20 °C:

$I(20\,^{\circ}C) = I(T)\left(\frac{293\,K}{T}\right)^2 e^{-\frac{E_g}{2k_B}\left(\frac{1}{293\,K}-\frac{1}{T}\right)}$, $E_g = 1.21\,\text{eV}$ (RD50 TN 2011-01)

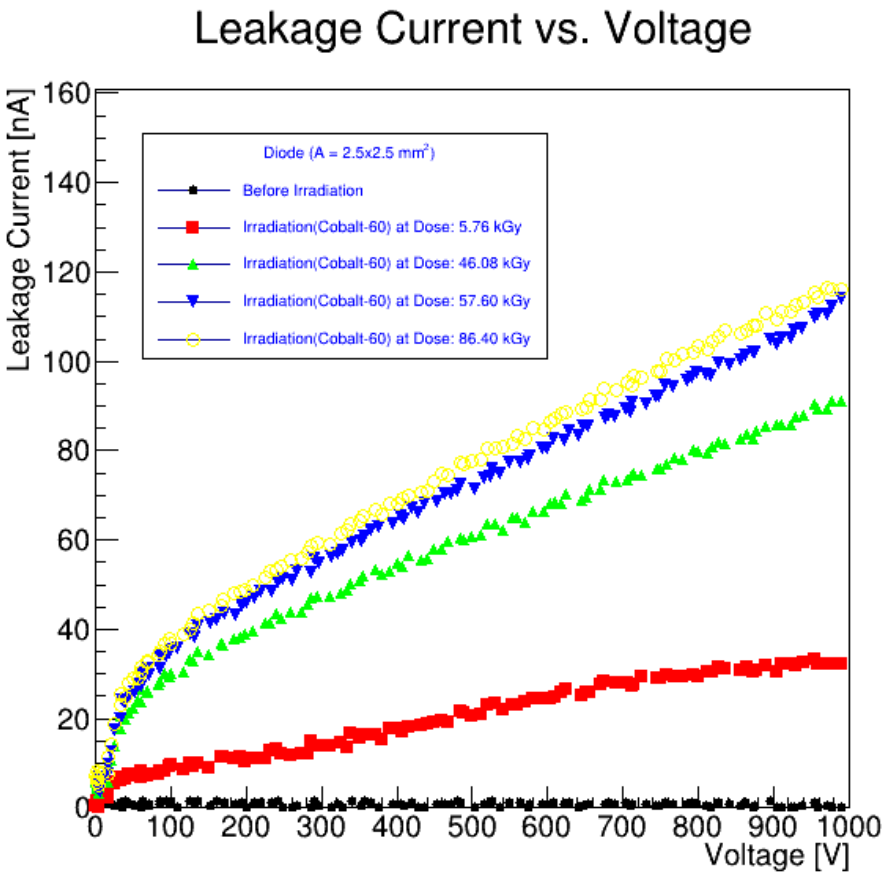

Annealing

Time lapses between two consecutive irradiation slots: $\sim$ 11 h - 15 h $\rightarrow$ the samples were stored at -28 °C

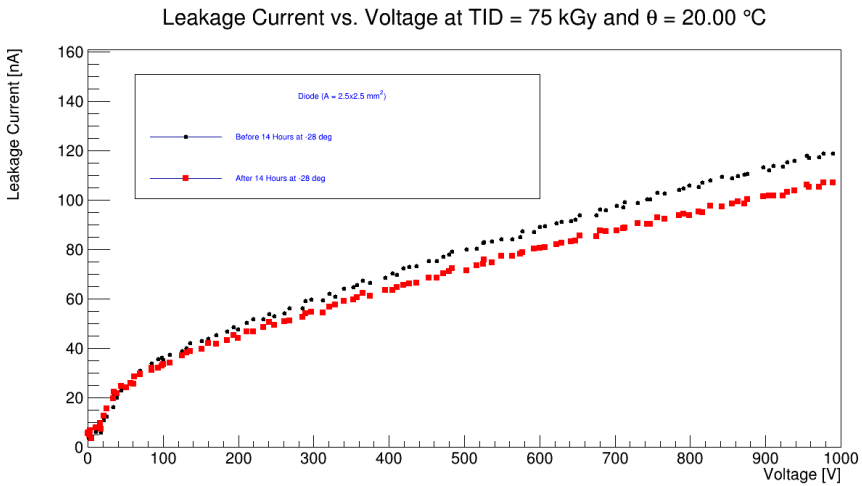

When measuring the IV after each period of storage in the freezer, annealing was observed every time

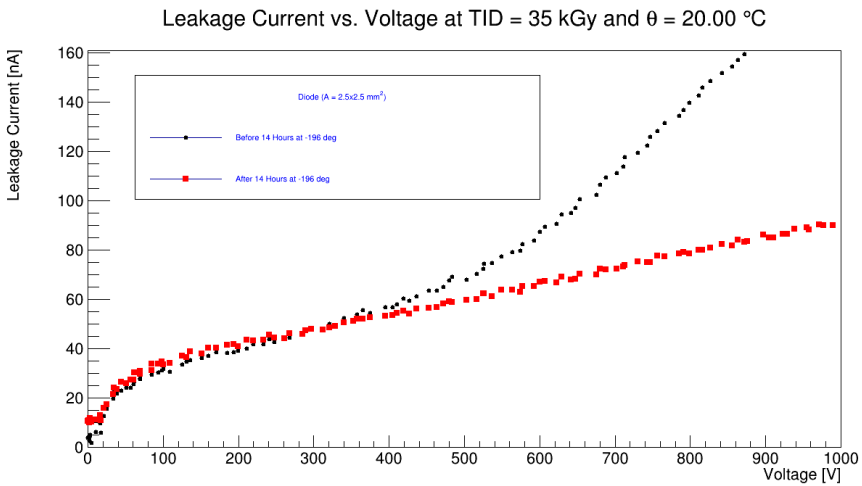

Annealing process was also observed after storage of the samples in a bottle of liquid N_2

Summary of the irradiation campaign

- Irradiation using ^{60}Co source of 11 TBq
- Total dose $\sim$86 kGy
- Irradiation of the MOS capacitor shows significant change in the flatband voltage, threshold voltage and depletion region slope (related to the charge concentration
- Diode CV measurements showed stable depletion voltage with dose as expected for oxygenated structures
- Diode IV measurements showed no breakdown behavior
- Annealing phenomena observed when using freezer at -28 °C to store sample between irradiation slots
- Phenomenon persisting also at -196 °C (liquid N_2)

The need for high-rate telescopes

- Extensive beam tests of the 2S modules are necessary (for channel efficiency, cluster size, cross talk between adjacent channels etc.)
- Existing telescopes used by CMS use a Monolithic Active Pixel Sensor chip with an integration time of 115.2 µs or 8.68 kHz readout frequency; integration time in Phase-2 Tracker modules (and other HL-LHC sensors) is 25 ns $\rightarrow$ 40 MHz ($\times$ 4600 the today's CMS telescopes readout frequency)
- We cannot test Phase-2 modules at nominal rates with the old telescopes used by CMS $\rightarrow$; that's why new high-rate telescopes are being developed, e.g. CHROMIE at CERN and CHROMini at IPHC-Strasbourg
- For CHROMIE see P. Asenov, Commissioning and simulation of CHROMIE, a high-rate test beam telescope, JINST 15 (2020) 02, C02003 and my dissertation

Description of the telescopes

- CHROMIE: particle rates up to 200 MHz/cm^2 (the highest rate of a Phase-2 Outer Tracker DUT: 50 MHz/cm^2); resolution of the order of 10-20 µm; pixel size: 100 × 150 µm^2; 8 layers, each containing two CMS Phase-1 BPIX modules (Grade C, active area of 2 × 16.2 × 64.8 mm^2) in a frame, 4 layers in front of the DUT, and 4 layers behind it; 20° tilt angle about x-axis; 30° skew angle about y-axis for all layers → to allow charge sharing between pixels; a block mounted on a carriage that can slide over rails holds each layer; auxiliary electronics mounted close to the modules, on the rails; 4 scintillators for triggering mounted on the rails; two in front of the layers, two behind it; actuators for DUT, translation in X/Y, rotation about X; CMS-standard readout system → SPS, 120 GeV π^+, 40 MHz
- CHROMini: very similar, but with only two planes and without any rotations of the planes → CYRCé, 25 MeV protons, 85 MHz time structure (can be made half with a kicker)

Visualization of the high-rate telescopes

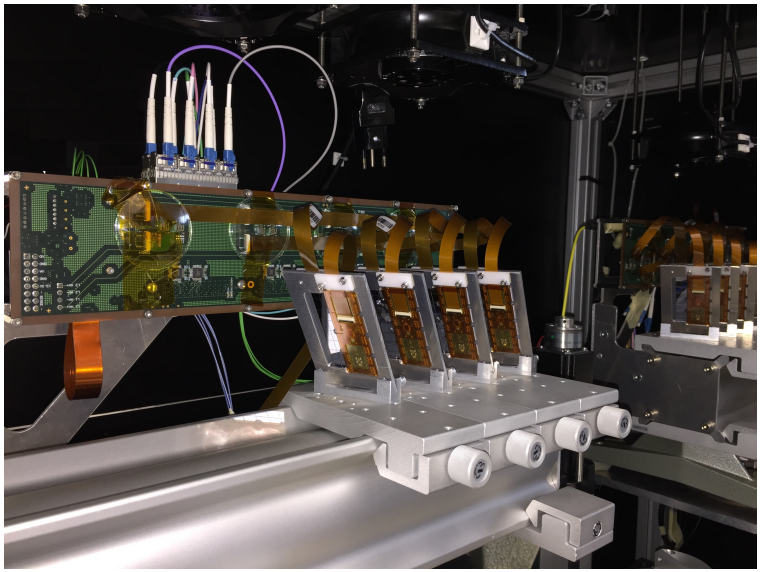

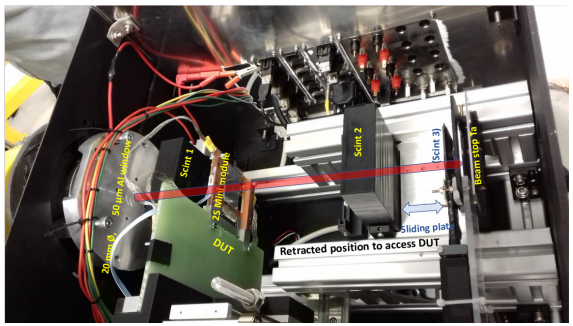

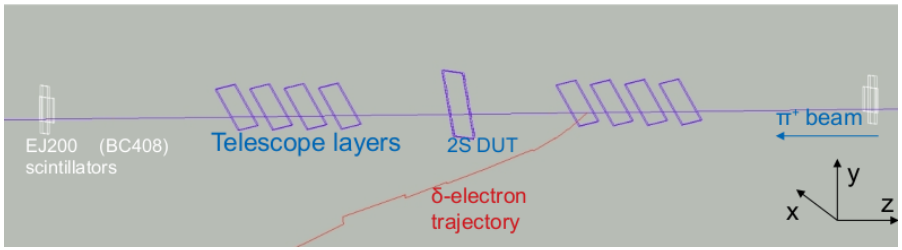

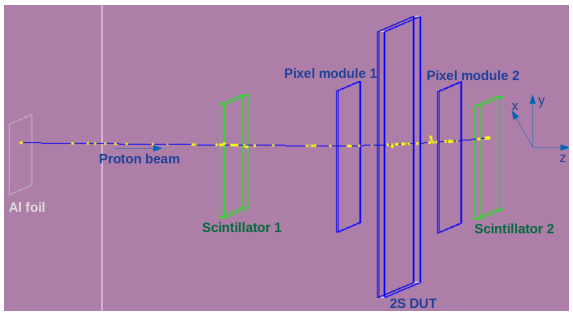

The CMS High Rate telescOpe MachInE (CHROMIE)

The CHROMini telescope (top: photo from IPHC)

Activities related to telescopes

- Pre-calibration of Phase-1 BPIX modules for CHROMIE with pXar
- Development of a standalone Geant4 simulation program for the operation of CHROMIE and CHROMini under beam
- Tracking/alignment algorithm for CHROMIE (CMSSW framework)
- Comparison between test beam data and simulation output

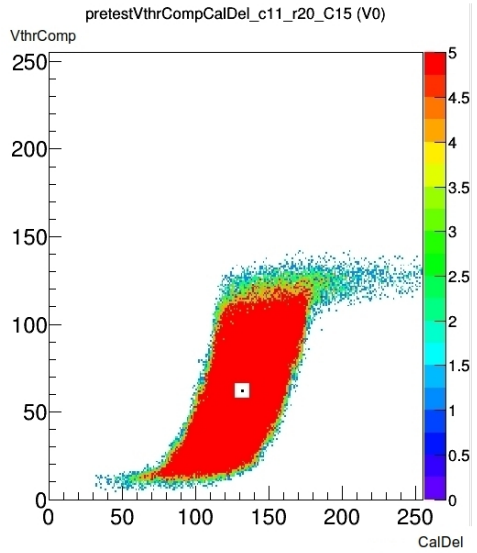

CalDel (delay of the pulse) versus VThrComp (global ROC threshold) $\rightarrow$ "Tornado plot"

The Geant4 standalone simulation programs

- Useful tools for the prediction of a pixel telescope behavior under beam
- In the case of CHROMIE $\rightarrow$ to give an indication of unknown beam parameters through comparison of its output with plots from real data where some magnitudes were unknown (e.g. beam size)
- In the case of CHROMini $\rightarrow$ during the design phase:
  - to show that the CHROMini project is feasible and can be used for tracking
  - to determine the optimal materials, thicknesses and pixel sizes, for various distances from the DUT, through different simulation runs
  - to estimate the DUT and telescope module residuals, as well as the angular straggling (for multiple scattering)
- These simulation programs could work as a potential basis for the study of pixel telescopes or experiments with similar strip/pixel modules

Simulation characteristics for CHROMini (1)

- 2S module DUT: 2 Si sensors (102700 μm $\times$ 94108 μm $\times$ 320 μm), with spacing between the sensors: $\sim$ 2 mm; strip pitch: 90 μm; active depth: 290 μm
- 2 pixel layer consisting of two Phase-1 BPIX modules each, one in front and one behind the DUT; BPIX module: 66.6 mm $\times$ 25 mm $\times$ 460 μm, 2 rows $\times$ 8 ROCs; pixel size: 150 μm $\times$ 100 μm
- A 50 μm thick Al foil at the beam line exit to separate the vacuum from the air
- A PVT (C_9H_{10}) scintillator of 2 mm thickness in front of the DUT and one similar scintillator behind the pixel layer, for triggering
- 25 MeV proton beam in z-direction
- Two scintillators, one before the first pixel ayer (along the way of the beam) and one behind the second pixel layer, used for triggering

Simulation characteristics for CHROMini (2)

- $z_0 = -23.5\,\text{cm}$ (the World boundary) $\rightarrow$ the z-positions of the centroids of each physical volume are: $z_0 + 7.6\,\text{cm}$ for the first scintillator, $z_0 + 11.7\,\text{cm}$ for the first pixel layer, $z_0 + 13.5\,\text{cm}$ for the 2S DUT, $z_0 + 15.3\,\text{cm}$ for the second pixel layer and $z_0 + 16.7\,\text{cm}$ for the second scintillator
- 20000 events for all plots presented below, except where mentioned otherwise
- Similar plots have been produced for CHROMIE

Physics processes

- Ionization
- Bremsstrahlung
- Pair production
- Annihilation
- Photoelectric effect
- γ-production
- Compton scattering
- Rayleigh scattering
- Klein-Nishina model for the differential cross section

General Particle Source (GPS) used instead of a particle gun (since it allows the specifications of the spectral, spatial and angular distribution of the primary source particles): position adjusted to the center of the beam from the data of a real run; only one pixel module hit
Circular beam: $\sigma_r = 2.123$ mm

Energy deposition per pixel/strip

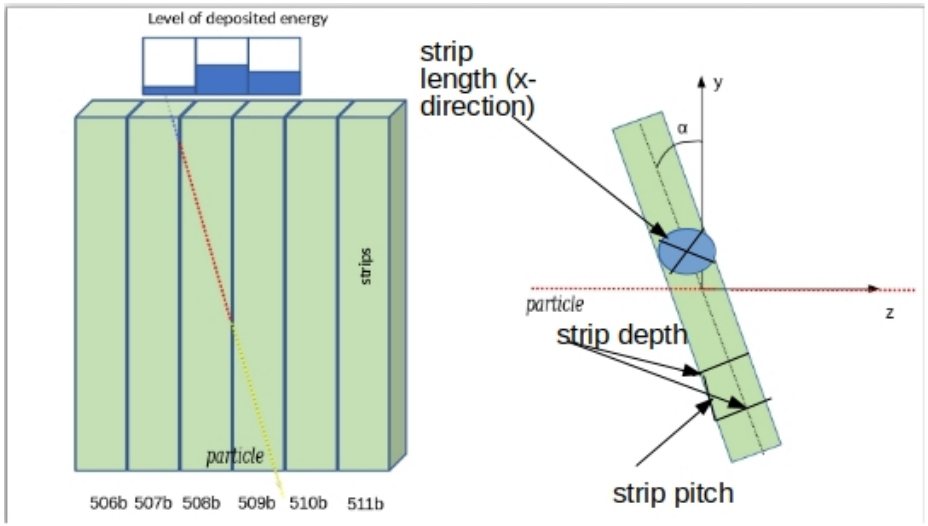

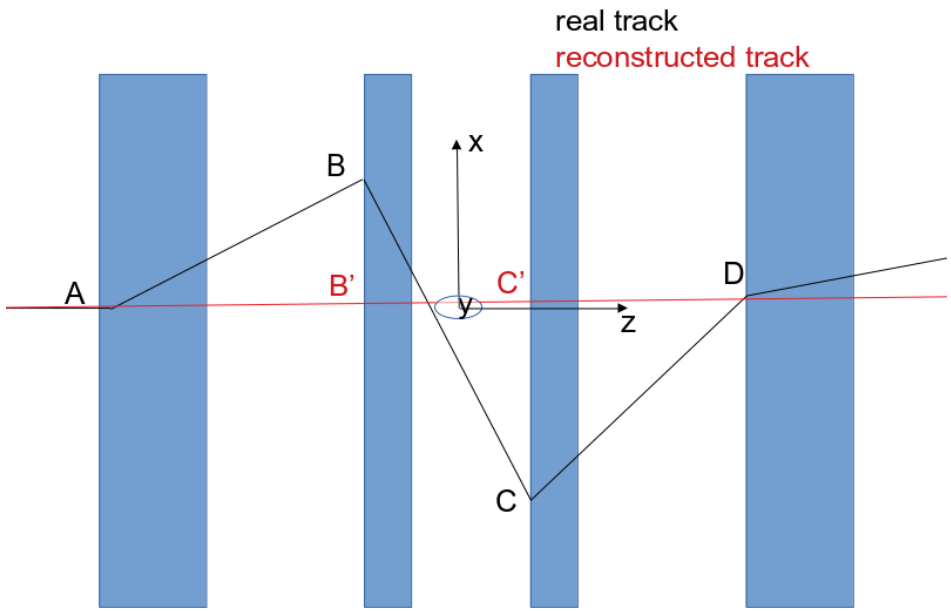

strip length // x-axis
strip pitch // y-axis

$$deflection\ angle = acos\left(\vec{u}_A \cdot \vec{u}_D\right), \vec{u}: momentum\ direction\ unit\ vector$$

Detector resolution

Determination of impact points:

$$R_{\text{pixel}} = \frac{1}{N_{\text{pixels}}} \sum_{i=1}^{N_{\text{pixels}}} w_{pi} P_{pi} \; R_{\text{strip}} = \frac{1}{N_{\text{strips}}} \sum_{i=1}^{N_{\text{strips}}} w_s P_{si} \qquad (1)$$

where N_{pixels} is the total number of pixels that have counted a hit in the current module, the weight $w_{pi} = \frac{\textit{charge collected in the } i-\textit{th pixel with a hit}}{\textit{total charge collected in all hit pixels in the current module}}$ and P_{pi} the geometrical center of the front surface (along the way of the beam) of the i-th pixel that has counted a hit in the current event; N_{strips} is the total number of strips that have counted a hit in the current sensor, the weight $w_s = \frac{1}{\textit{number of hit strips in the current sensor}}$ and P_{si} the geometrical center of the front surface (along the way of the beam) of the i-th strip that has counted a hit

Detector residuals: Calculation

Calculation of residuals:

$$\vec{r}_{AD} = \vec{r}_D - \vec{r}_A = (x_{AD}, y_{AD}, z_{AD}) \tag{2}$$

$$\frac{x - x_A}{x_{AD}} = \frac{y - y_A}{y_{AD}} = \frac{z - z_A}{z_{AD}} \tag{3}$$

$$z_{B'} = z_B,\ z_{C'} = z_C \tag{4}$$

$$x_{B'} = x_{AD}\frac{z_B - z_A}{z_{AD}} + x_A,\ x_{C'} = x_{AD}\frac{z_C - z_A}{z_{AD}} + x_A \tag{5}$$

$$y_{B'} = y_{AD}\frac{z_B - z_A}{z_{AD}} + y_A,\ y_{C'} = y_{AD}\frac{z_C - z_A}{z_{AD}} + y_A \tag{6}$$

$$s_{1x} = x_B - x_{B'},\ s_{1y} = y_B - y_{B'},\ s_{2x} = x_C - x_{C'},\ s_{2y} = y_C - y_{C'} \tag{7}$$

Residuals and deflection angle

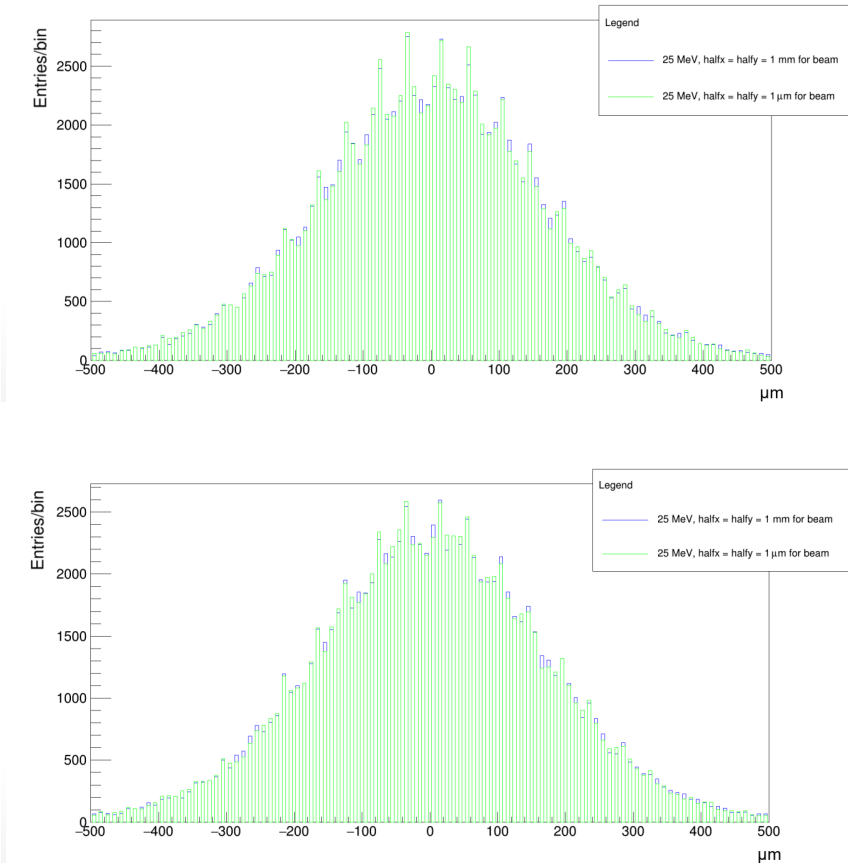

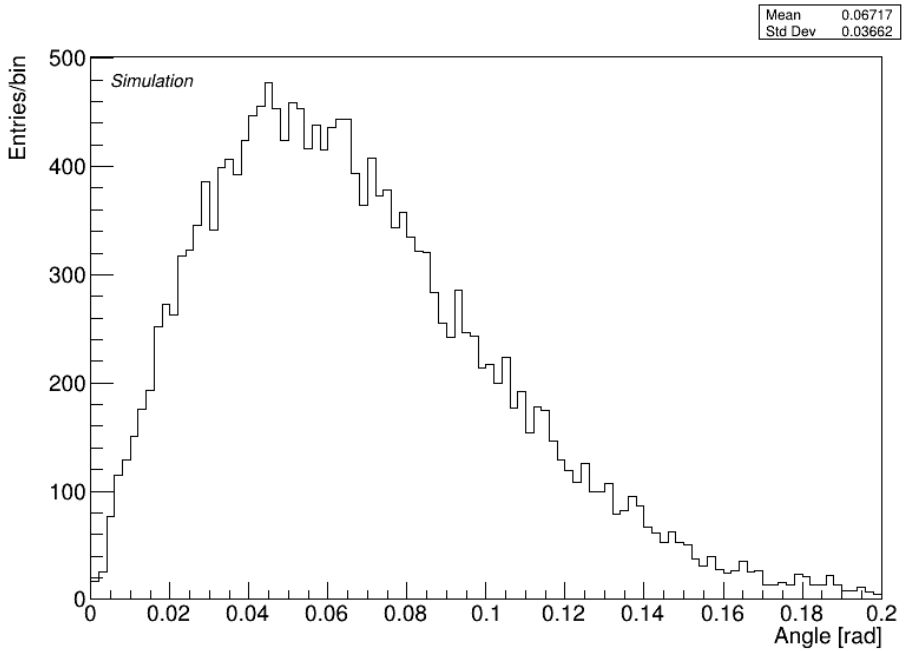

Y-residuals for the first 2S sensor ($B^{'}B_y$) and the second 2S sensor ($C^{'}C_y$) along the way of the beam

Deflection angle:

$$\theta_d = \arccos\left(\vec{u}_A \cdot \vec{u}_D\right)$$

Energy deposited in the various volumes of the geometry

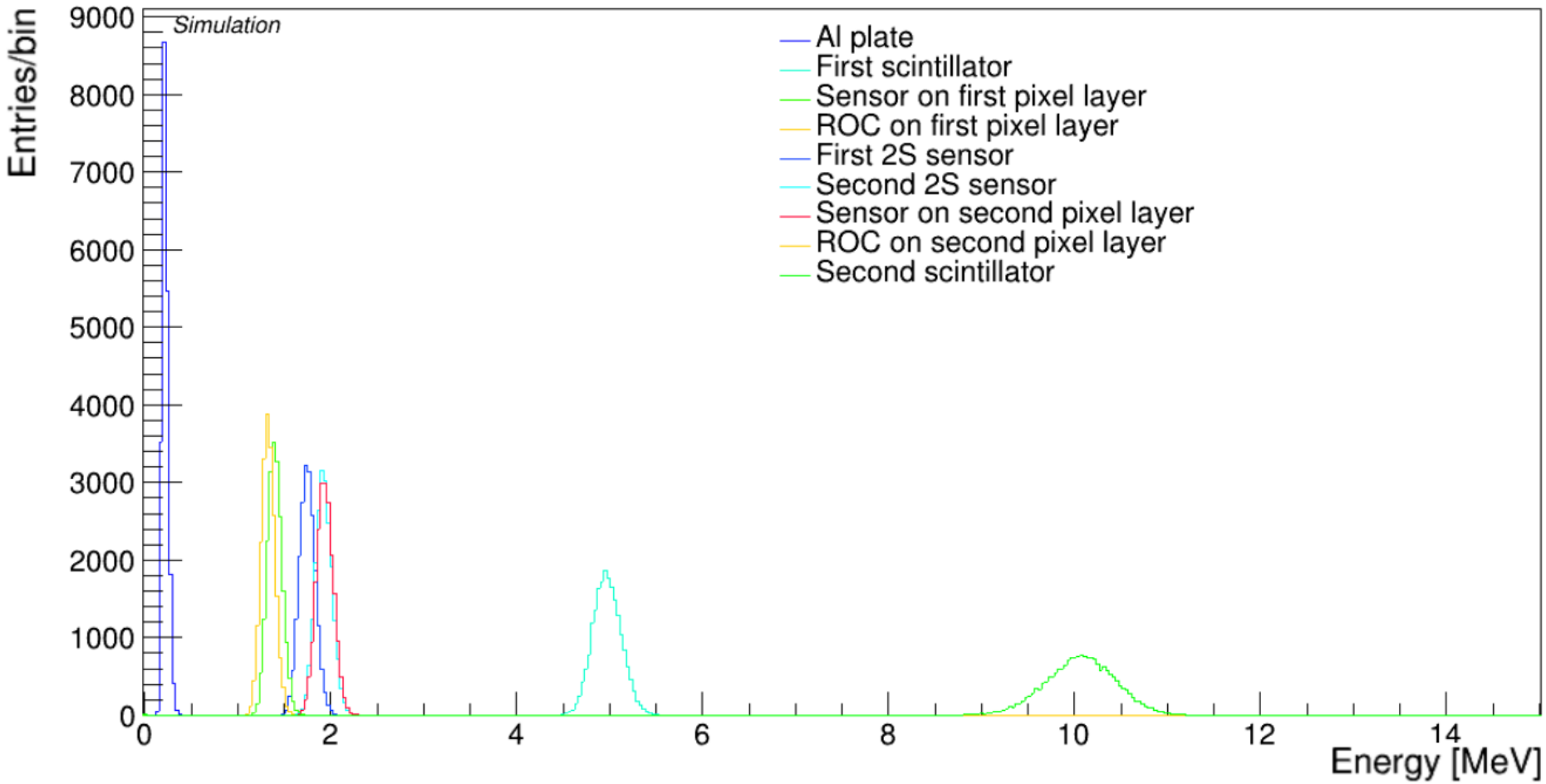

Kinetic energy of a primary proton vs. z for a single event

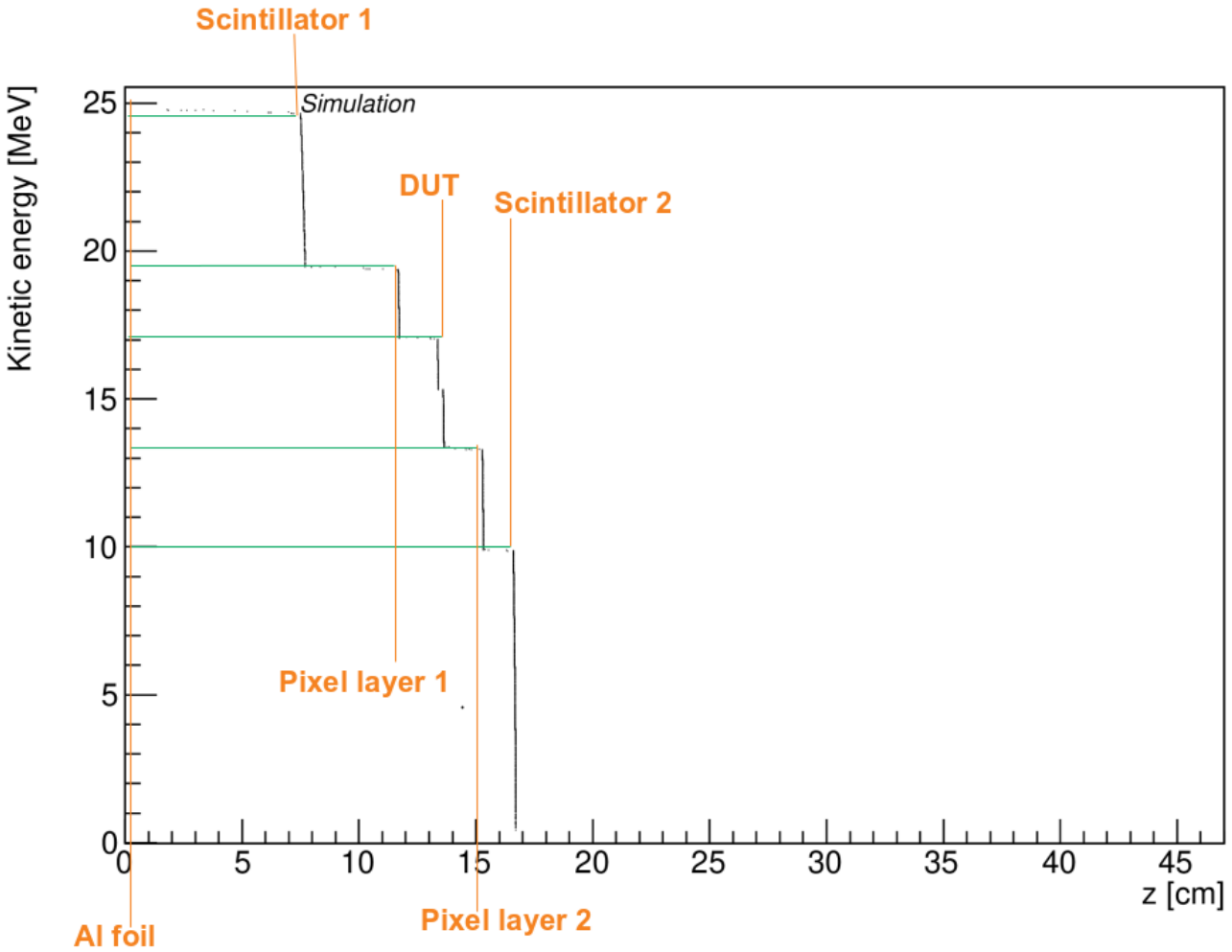

Other output of the simulation

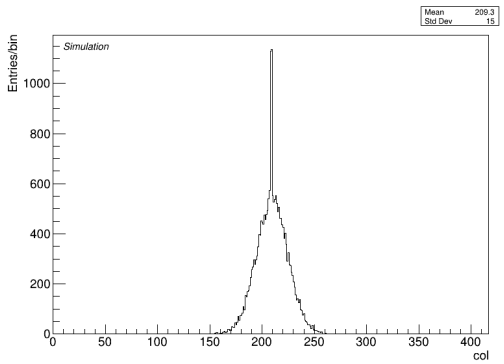

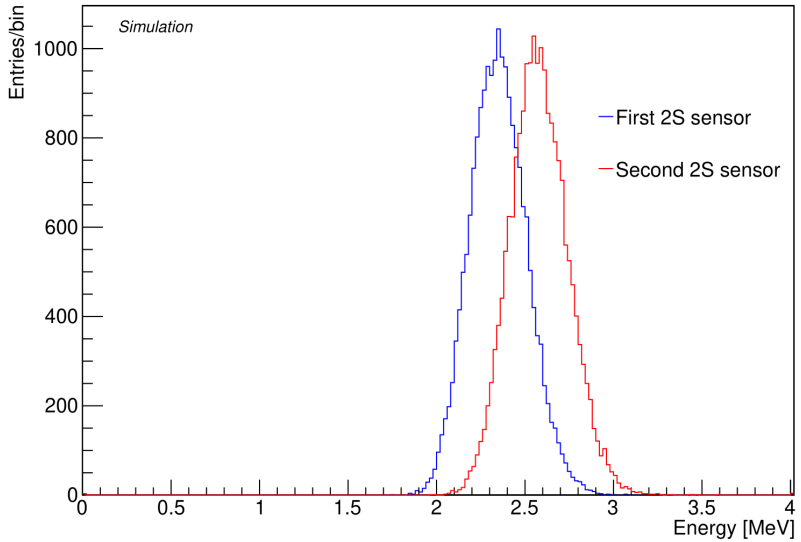

Total energy lost by the primary protons in the 2S sensors

Projected hit maps along columns and along rows for the hit module of the 2nd pixel layer along the way of the beam

Hit map: comparison with test beam data from IPHC

Hit occupancy per column per row for the hit module of the second pixel layer; the module is operated at a depletion voltage of $-100\,\mathrm{V}$

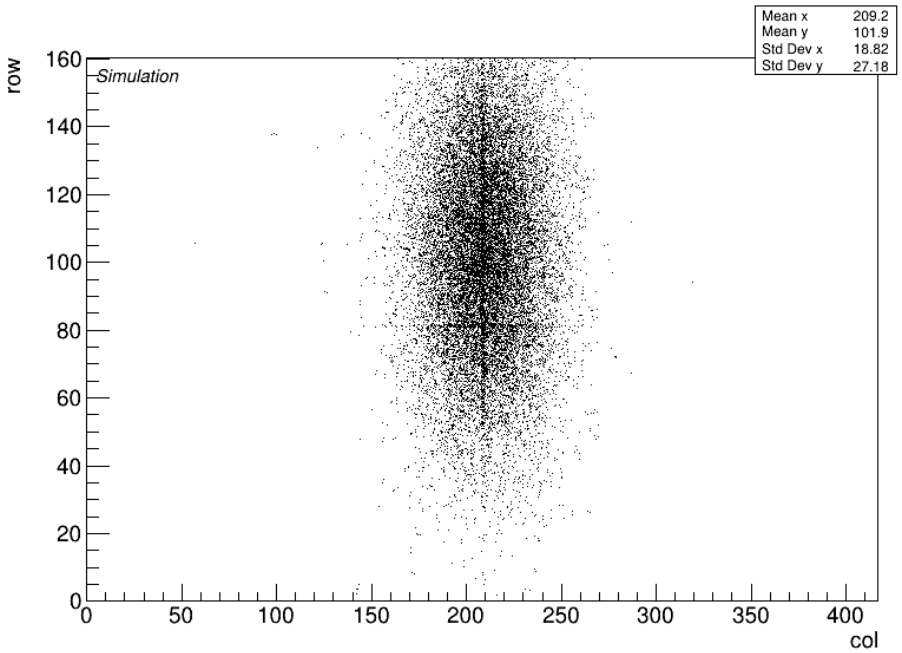

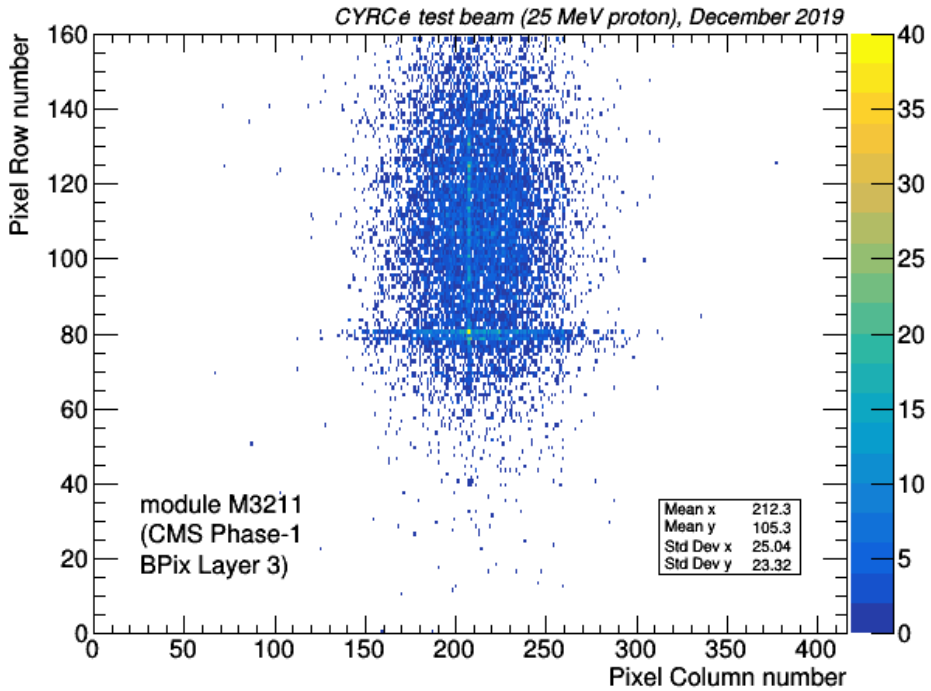

CHROMIE: hit positions (Layer 2)

Hit positions per column per row for the left module of Layer 2 for a 120 GeV π^+ beam (beam diameter = 15 mm and σ_E = 100 keV)

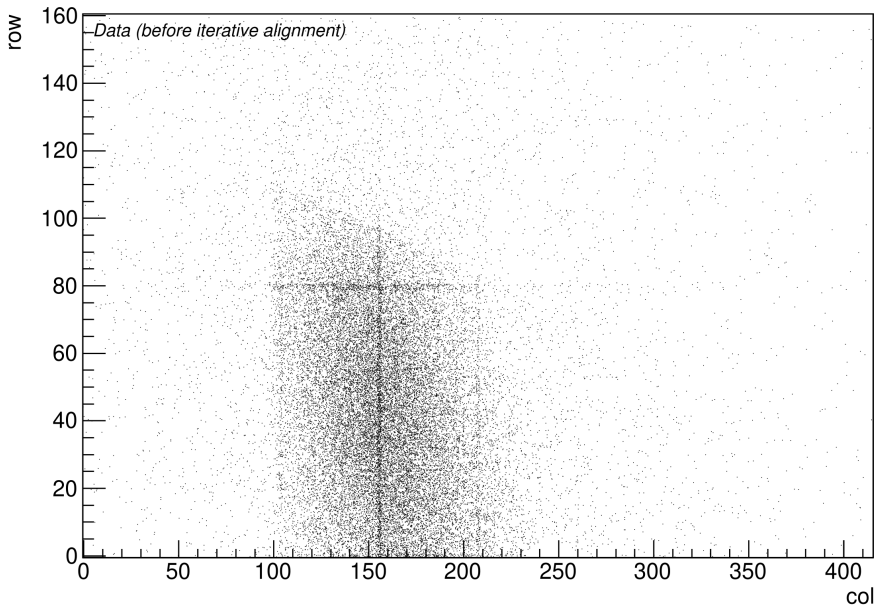

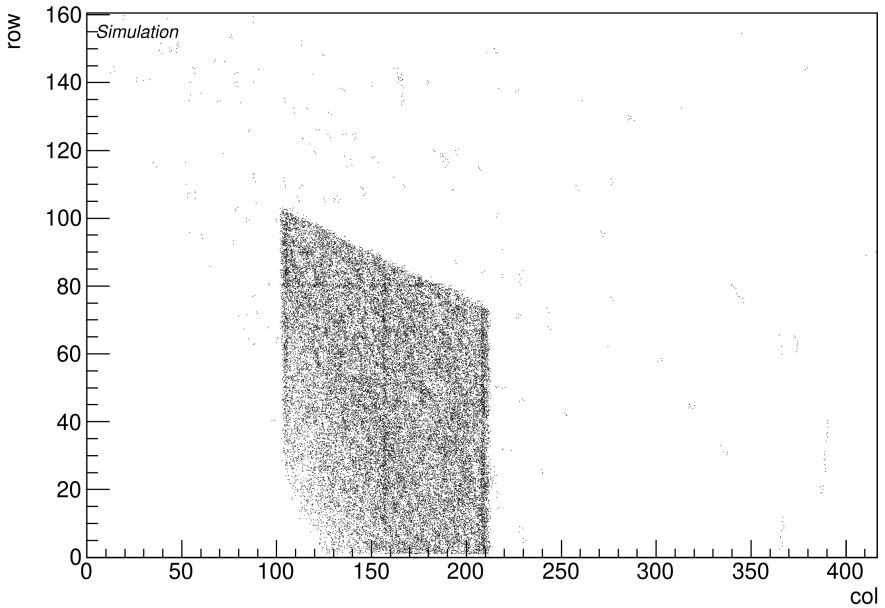

Test beam characterization of a 2S module

- TB21, DESY, October-November 2019; 4 GeV electrons; 2S modules as DUT produced at KIT, RWTH-Aachen, Brown University
- DATURA telescope
  - EUDET-type
  - 6 pixel detector planes equipped with MIMOSA 26
  - pixels sized 18.4 μm $\times$ 18.4 μm, arranged in 1152 columns and 576 rows
  - sensors thinned down to a thickness of about 50 μm and together with 50 μm of thin protective lightproof Kapton foil (25 μm on each side of a sensor)
- Goals: verification of the uniformity of efficiencies; check for inefficiencies or hit/stub duplications in the center of a 2S; check stub finding inefficiency for tracks inclined along the strips; measurement of efficiency and noise hit rate versus the threshold...

The initial configuration

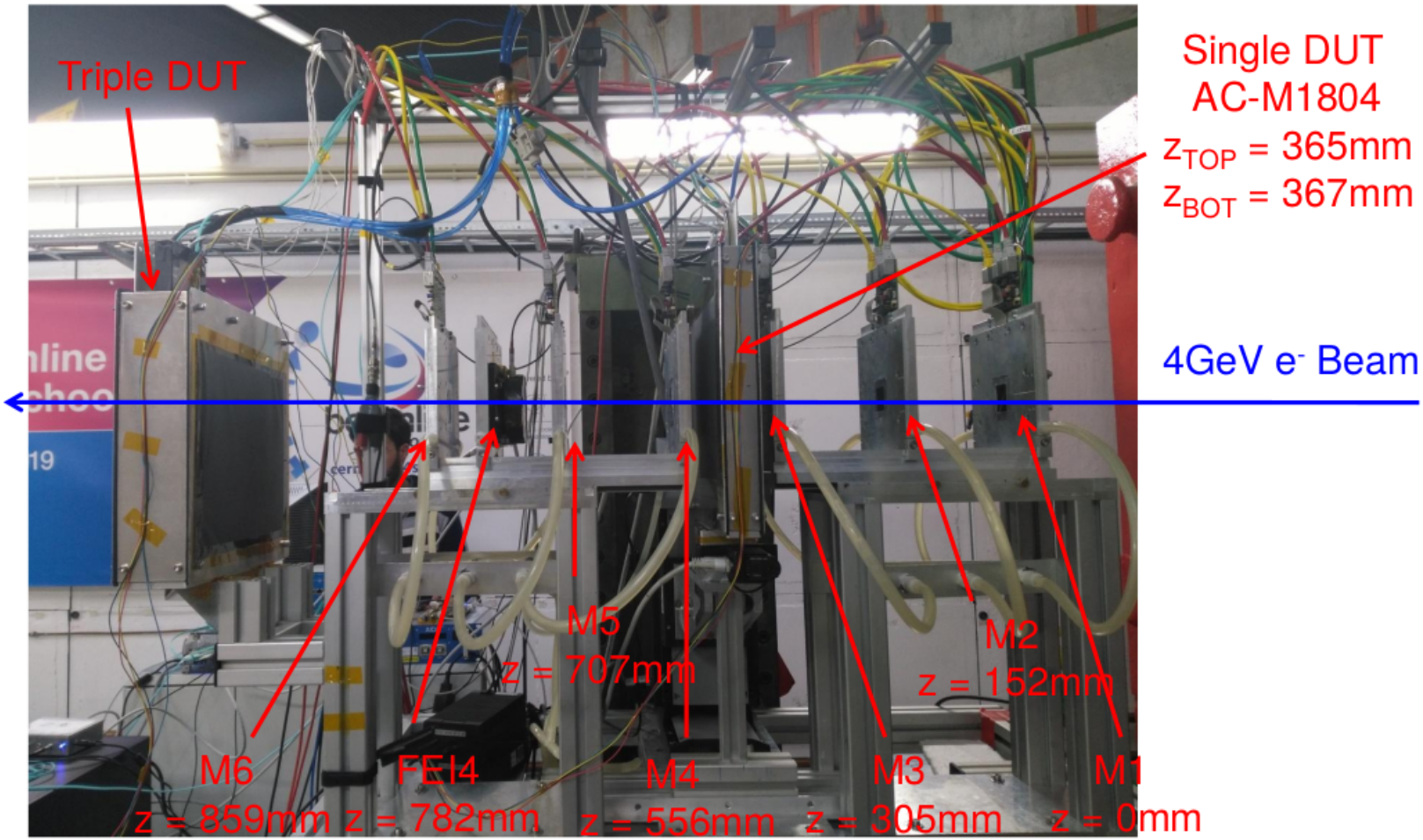

Data analysis

Data analysis performed either within the scope2s framework (developed mostly by DESY members) or within the EUTelescope framework (developed mostly by KIT members)
Goal of our group: to calculate the stub efficiency for various configurations
Event selection:

1. Reconstruct clusters in the six DATURA planes
2. Fit a track with the fist three DATURA planes
3. Fit a track with all the six DATURA planes
4. If a track that fulfills the above conditions is found then:
   1. Reconstruct cluster in both DUT planes
   2. Declare a cluster-track match if $|\Delta x_{\mathrm{cluster-track}}| < 0.1\,\mathrm{mm}$
   3. Check if a stub exists, and if it does declare a stub-track match if $|\Delta x_{\mathrm{stub-track}}| < 0.2\,\mathrm{mm}$

Stub efficiency for an angular scan (scope2s)

After the end of each run, the number of cluster-track matches Q_1 and the number of stub-track matches Q_2 are printed out $\rightarrow$ the stub efficiency is defined as Q_2/Q_1

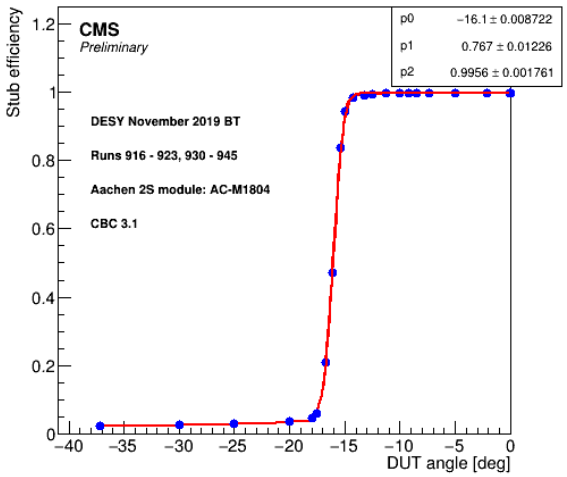

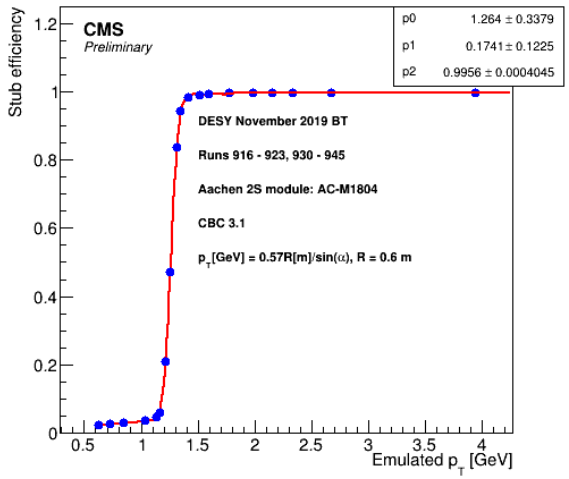

scope2s used for the analysis
Rotations about the y-axis
$V_{bias} = -300\text{V}$
Fit performed using a generic FCN function

$$p_{\mathrm{T}}[GeV] = 0.57 \cdot \frac{R[\mathrm{m}]}{sin(\alpha)},\ R = 0.6\,\mathrm{m}$$

Tracks inclined along the strips (scope2s)

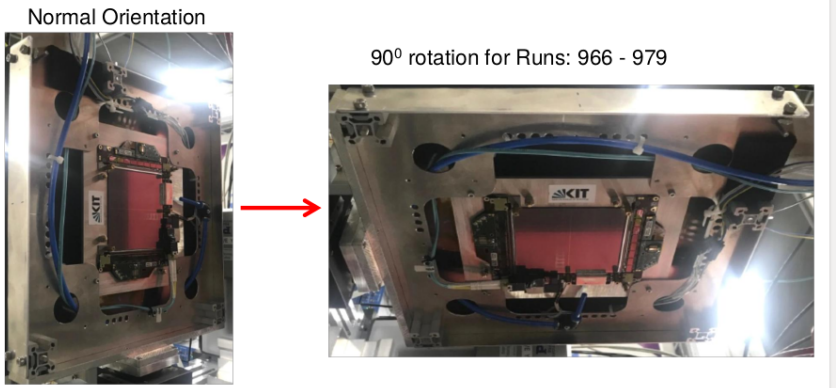

Before, the length of the strips was along the y-axis (vertical axis), here it was along the x-axis (horizontal axis)
Steady $x = 114.662\,\text{mm}$ and $y = 47.278\,\text{mm}$ and rotations about the y-axis

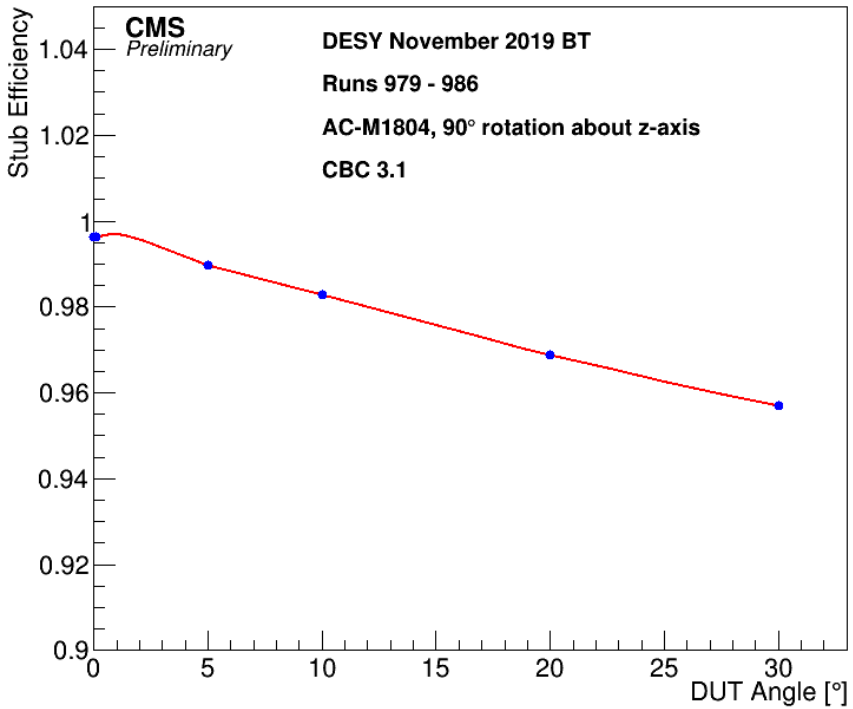

Summary

- Irradiation campaign with ^{60}Co γ-photons and subsequent electrical characterization showed that a few hours of annealing are enough to decrease the leakage current of the sensors; leakage current of the order of 100 nA even after $\sim$ 90 kGy of irradiation; proven suitability of the devices for high-luminosity applications
- Standalone simulation programs for pixel telescope operation under various types of beam $\rightarrow$ can be used for the design of future pixel telescopes or tracker systems
- Stub efficiency of a 2S module determined for a classic angular scan and an angular scan along the strips

References (1)

P. Asenov, Commissioning and simulation of CHROMIE, a high-rate test beam telescope, JINST 15 (2020) 02, C02003.
P. Asenov, P. Assiouras et al., Cobalt-60 gamma irradiation of silicon test structures for high-luminosity collider experiments, PoS Vertex2019 (2020) 061.
P. Assiouras, P. Asenov et al., A program for fast calculation of capacitances, in planar pixel and strip silicon sensors, PoS Vertex2019 (2020) 059.
CMS collaboration, The phase-2 upgrade of the CMS tracker, CERN, Geneva, Switzerland, Rep. CERN-LHCC-2017-009.
W Adam et al., P-type silicon strip sensors for the new CMS Tracker at HL-LHC, JINST 12 (2017) 06, P06018.
W Adam et al., Characterisation of irradiated thin silicon sensors for the CMS phase II pixel upgrade, Eur.Phys.J.C 77 (2017) 8, 567.

References (2)

W Adam et al., Beam test performance of prototype silicon detectors for the Outer Tracker for the Phase-2 Upgrade of CMS, JINST 15 (2020) 03, P03014.

P. Asenov, Test beam facility at CYRCé for high particle rate studies with a CMS upgrade module: design and simulation, 7th Beam Telescopes and Test Beams Workshop, 14-18 January 2019, CERN.

P. Asenov, Contribution of INPP to the CMS Phase-2 Upgrade, HEP 2019 - Conference on Recent Developments in High Energy Physics and Cosmology 17-20 April 2019, NCSR "DEMOKRITOS", Athens, Greece.

P. Asenov, Performance of a simple 2-plane telescope (CHROMini) and a CMS 2S module in a 25 MeV proton beam: Comparison between data and Geant4 simulation, 8th Beam Telescopes and Test Beams Workshop, 27-31 January 2020, Tbilisi State University.

Backup

Properties of silicon

$$f(E) = \frac{1}{e^{\frac{E-E_F}{k_B T}} + 1} \tag{8}$$

$$n = N_C e^{-\frac{E_C - E_F}{k_B T}} \tag{9}$$

$$p = N_V e^{-\frac{E_F - E_V}{k_B T}} \tag{10}$$

$$N_C = 2\left(\frac{2\pi m_e^* k_B T}{h^2}\right)^{\frac{3}{2}} \tag{11}$$

$$N_V = 2\left(\frac{2\pi m_h^* k_B T}{h^2}\right)^{\frac{3}{2}} \tag{12}$$

$$n_i = \sqrt{np} = n = p = \sqrt{N_C N_V} e^{-\frac{E_G}{2k_B T}} \tag{13}$$

p-n diode (1)

$$J_p = J_{p,\,Drift} + J_{p,\,Diffusion} = q\mu_p pE - qD_p \nabla p \tag{14}$$

$$J_n = J_{n,\,Drift} + J_{n,\,Diffusion} = q\mu_n nE + qD_n \nabla n \tag{15}$$

$$J = J_p + J_n \tag{16}$$

$$V_{bi} = V_T \ln\left(\frac{N_D N_A}{n_i}\right) \tag{17}$$

$$V = V_a - V_{bi} \tag{18}$$

$$x_d = x_n + x_p \tag{19}$$

$$Q_n = qN_D x_n \tag{20}$$

$$Q_p = -qN_A x_p \tag{21}$$

p-n diode (2)

$$x_d = \sqrt{\frac{2\epsilon_s}{q}\left(\frac{1}{N_A}+\frac{1}{N_D}\right)(V_{bi}-V_a)} \tag{22}$$

$$x_n = \sqrt{\frac{2\epsilon_s}{q}\frac{N_A}{N_D}\frac{1}{N_A+N_D}(V_{bi}-V_a)} \tag{23}$$

$$x_p = \sqrt{\frac{2\epsilon_s}{q}\frac{N_D}{N_A}\frac{1}{N_A+N_D}(V_{bi}-V_a)} \tag{24}$$

$$C_j = \sqrt{\frac{q\epsilon_s}{2(V_{bi}-V_a)}\frac{N_A N_D}{N_A+N_D}},\ C_j = \frac{\epsilon_s}{x_d} \tag{25}$$

$$\rho = \frac{1}{q(n\mu_n + p\mu_p)} \tag{26}$$

MOS capacitor

$$V_{FB} = \Phi_{MS} - \frac{Q_i}{C_{ox}} - \frac{1}{\epsilon_{ox}} \int_0^{t_{ox}} \rho_{ox}(z) z dz \tag{27}$$

$$Q_d = -qN_A x_d \tag{28}$$

$$E_s = \frac{qN_A x_d}{\epsilon_s} \tag{29}$$

$$V_T = V_{FB} + 2\phi_F + \frac{\sqrt{4\epsilon_s qN_A \phi_F}}{C_{ox}} \tag{30}$$

$$C_{FB} = \frac{1}{\frac{1}{C_{ox}} + \frac{L_D}{\epsilon_s}} \tag{31}$$

$$L_D = \sqrt{\frac{\epsilon_s V_T}{qN_A}} \tag{32}$$

Particle-matter interaction

$$\left\langle -\frac{dE}{dx} \right\rangle = Kz^2 \frac{Z}{A} \frac{1}{\beta^2} \left[\frac{1}{2} \ln \left(\frac{2m_e c^2 \beta^2 \gamma^2 W_{max}}{I^2} \right) - \beta^2 - \frac{\delta(\beta\gamma)}{2} \right] \quad (33)$$

$$W_{max} = \frac{2m_e c^2 \beta^2 \gamma^2}{1 + 2\gamma \frac{m_e}{M} + \left(\frac{m_e}{M}\right)^2} \quad (34)$$

$$\frac{\Delta I_{vol}}{V} = \alpha \Phi \quad (35)$$

Silicon sensors as particle detectors

$$i = qvE_v \tag{36}$$

$$ENC = \sqrt{ENC_{C_d}^2 + ENC_{I_L}^2 + ENC_{R_P}^2 + ENC_{R_S}^2} \tag{37}$$

$$\Delta_p = \xi \left[\ln\left(\frac{2mc^2\beta^2\gamma^2}{I}\right) + \ln\left(\frac{\xi}{I}\right) + j - \beta^2 - \delta(\beta\gamma) \right] \tag{38}$$

where $\xi = (K/2)\langle Z/A \rangle z^2(x/\beta^2)$ and $j = 0.2$

$$x = \frac{p}{\sqrt{12}} \tag{39}$$

V_{FB} - N_{oxide} relation

V_{FB} can be expressed as a sum of: the difference between work functions of metal and semiconductor (which remains stable), the voltage across the oxide due to the charge at the oxide-semiconductor interface and a third term which is due to N_{oxide}

2.5 mm sized (half) diode: CV measurements

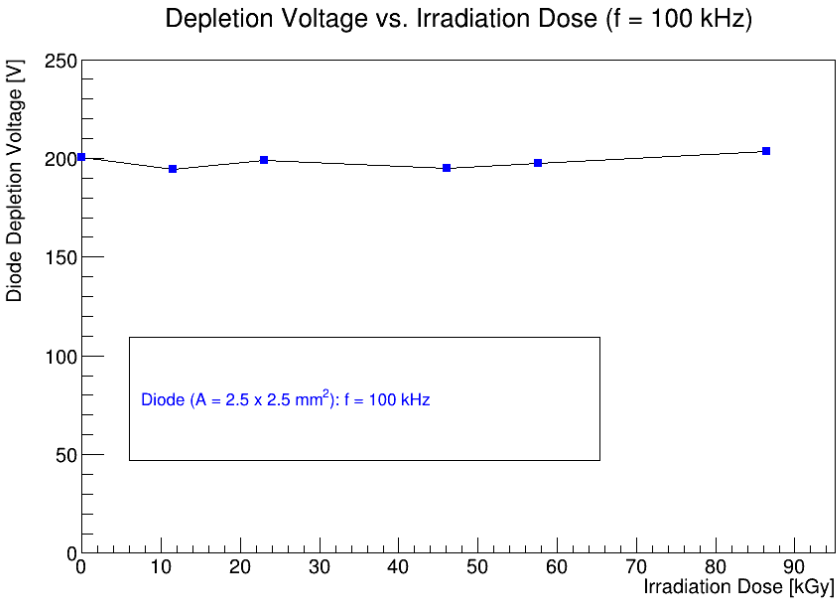

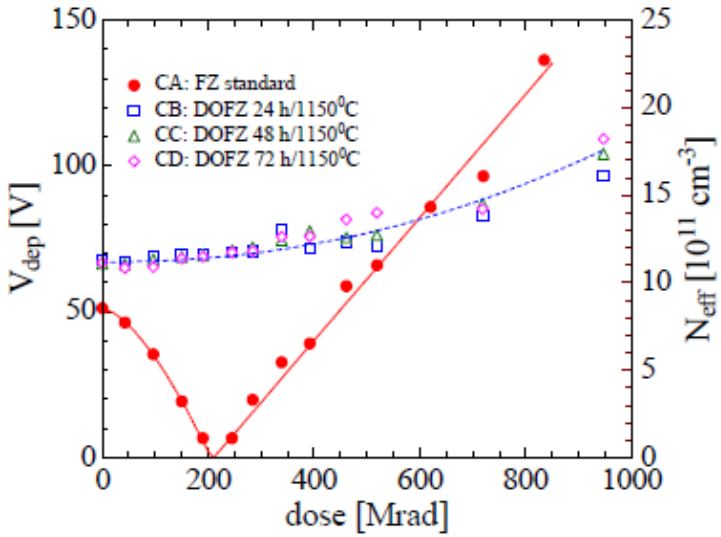

Gunnar Lindström, Radiation Damage in Silicon Detectors, Nucl. Instr. and Meth. A.

The Phase-1 BPIX sensor geometry

Sensor silicon area 18.6x66.6mm^2
Number of ROCs=2x8
Pixel size 100x150um^2 (size twice as wide at chip boarders)
Number of pixels 80x52
Sensor active area 16.2x64.8mm^2 since
2*(80*0.1mm+0.1mm)=16.2mm
8*(52*0.15mm+2*0.15mm)=64.8mm

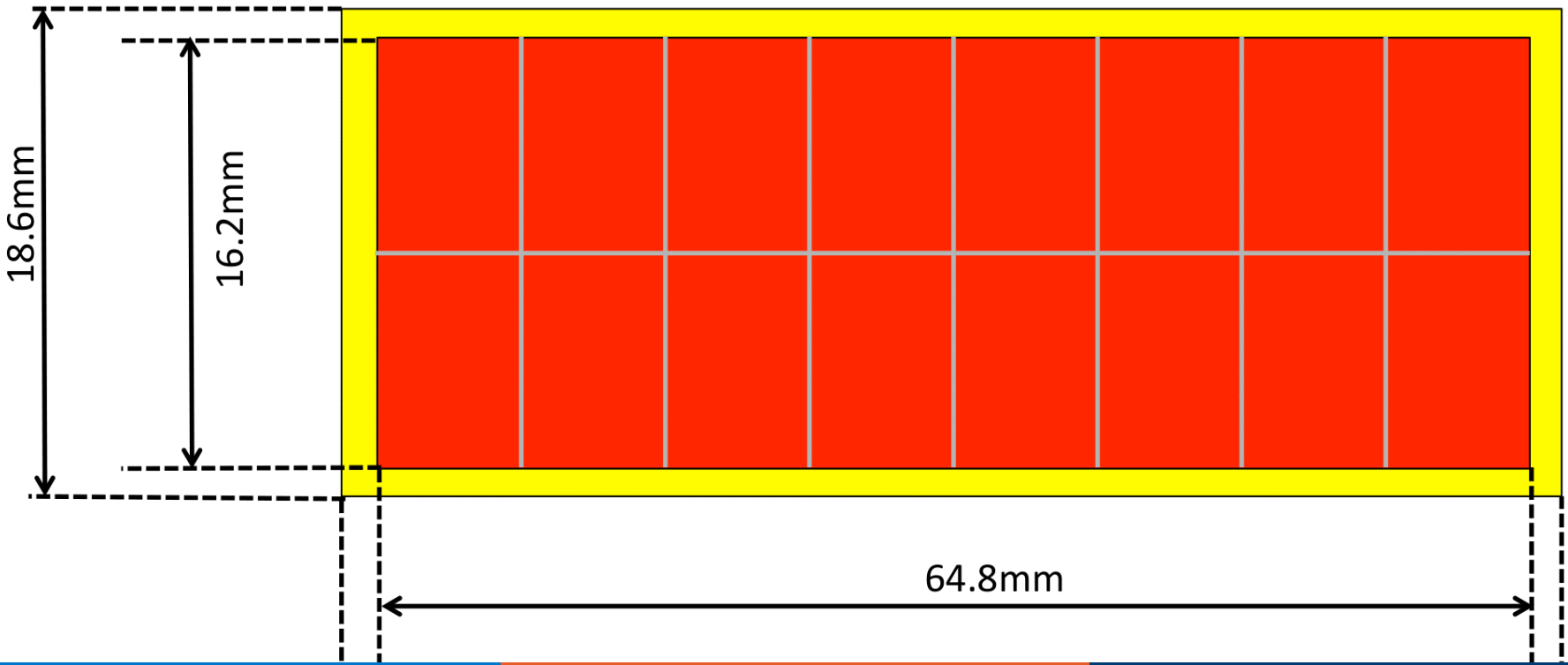

CHROMIE: Tracking

- Tracking strategy:
  - Removing noisy channels
  - Applying a coarse alignment (demanding that all tracks should be parallel to the beam axis)
  - Seeding
  - Pattern recognition
- Seeding: a search (conducted using global coordinates) for 2 points, one in Seeding Layer 1 and one in Seeding Layer 2, with $\Delta x < 0.1\,\text{cm}$ and $\Delta y < 0.1\,\text{cm}$ (corrected for misalignment: translation on x-axis + $50\,\text{cm} \rightarrow$ a new (0, 0, 0) point); loop on the clusters of the seeding modules
  - First check L1-L2, then L2-L3, then L3-L4, until a seed is found. (The layers on the arm of CHROMIE behind the DUT, on the way of the beam, weren't used because two dead and one noisy modules are located there.)

CHROMIE: analysis results

- Pattern recognition: look for the cluster with the smallest 2D distance from the track within the telescope layer $\rightarrow$ fit the track including the new cluster in the list, minimizing the 2D distance in the telescope layer
- Short tracks (that not hit at least 4 modules) are not considered valid tracks
- Seeding efficiency: 78.7%. Note: In our run analysis:
  - (Number of events with at least 4 layers with at least one cluster and 0 seeds)/(Number of events with at least 4 layers with at least one cluster) = 6082/28551 = 21.3%
  - Number of events with 0 layers with at least 1 cluster = 1015 $\rightarrow$ 1015/32536 = 3.12% of the total events $\rightarrow$ upper limit for efficiency is 96.88%

CHROMIE residuals (Layer 3)

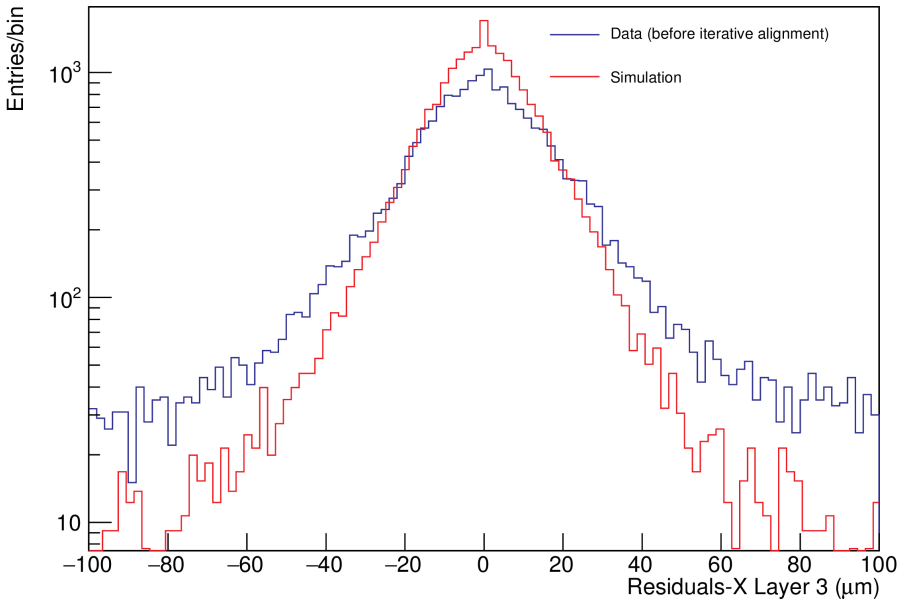

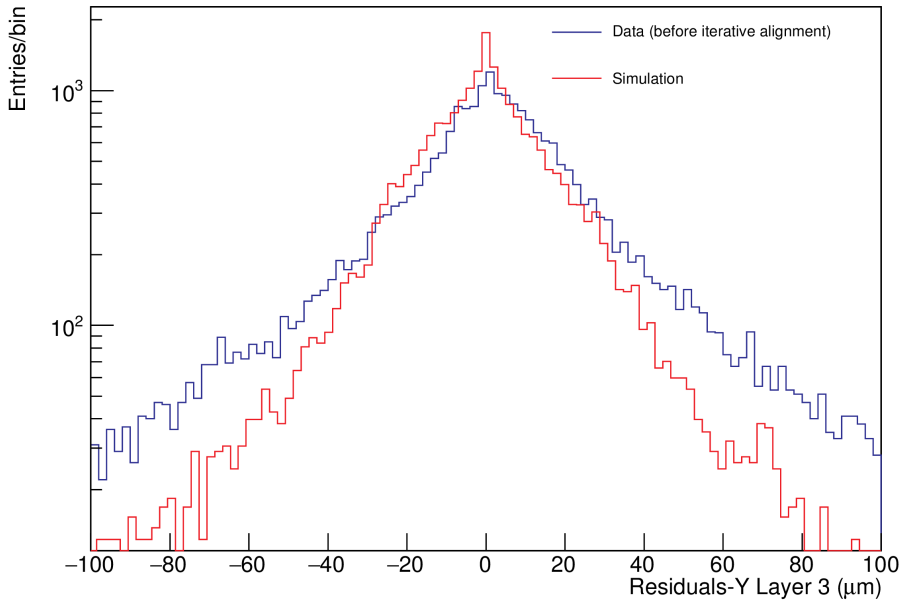

CHROMIE: cluster size

Table 5.5: Mean value of cluster size in the x-direction for CHROMIE; comparison between beam test data and simulation.

CHROMIE layer (only left modules are hit)	1	2	3	4	5	6	7	8
Mean value of cluster size-X (in pixels; beam test)	1.983	1.937	1.973	1.469	1.899	-	-	1.991
Mean value of cluster size-X (in pixels; simulation)	1.639	1.642	1.649	1.653	1.658	1.661	1.664	1.669

Table 5.6: Mean value of cluster size in the y-direction for CHROMIE; comparison between beam test data and simulation.

CHROMIE layer (only left modules are hit)	1	2	3	4	5	6	7	8
Mean value of cluster size-Y (in pixels; beam test)	1.695	1.736	1.730	1.355	1.718	-	-	1.754
Mean value of cluster size-Y (in pixels; simulation)	1.577	1.583	1.594	1.599	1.598	1.603	1.603	1.608

CHROMini: kinetic energy of a primary proton vs. z

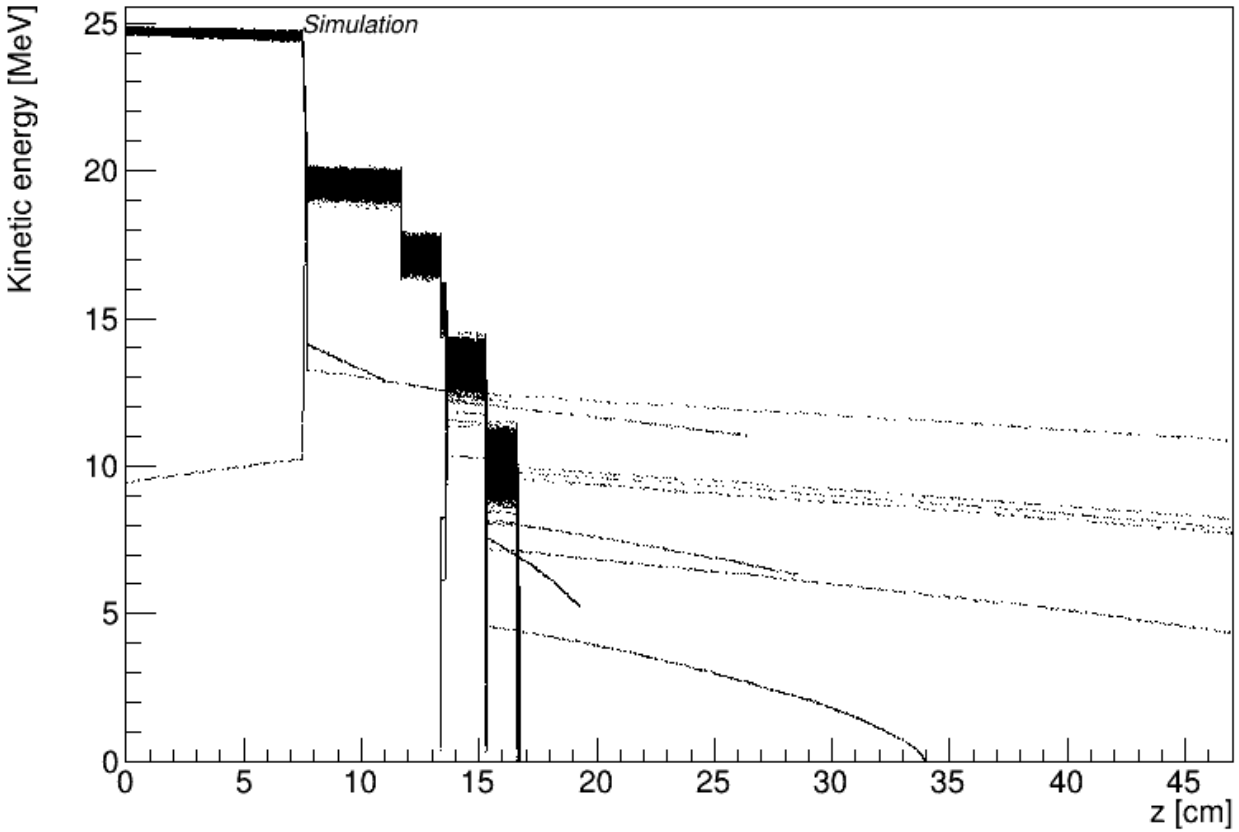

Basic difference between EUTelescope and scope2s frameworks regarding the stub efficiency

- EUTelescope compares a track directly to the stub, without any selection based on the hits, and thus examines the efficiency of the full 2S module to produce a stub for a given incident track
- scope2s uses only tracks that are matched to hits in each of the sensors of the 2S module, and thus checks that the CBC stub correlation logic is working as expected

When the DUT is rotated, the displacement between the hits in the two sensors of the 2S module becomes larger, and at a certain angle the number of stubs is expected to decrease $\rightarrow$ in case that a hit is lost by one of the sensors and no stub is created, in the EUTelescope approach this would be counted as an inefficient event, while in the scope2s approach it would not be counted at all and the event wouldn't be included in the analysis

DATURA alignment

Each sensor plane defines a local coordinate systems for its hits (columns and rows for pixels; rows for strips). The second telescope plane defines the global xy reference system. The beam is along the z-axis, and the tracks of the primary particles are straight since there is no magnetic field present in the telescope system. The alignment is hierarchical: the 1st and 3rd telescope planes are aligned relatively to the 2nd (x- and y-shifts and rotation), the 4th and 6th telescope planes are aligned relatively to the 5th (x- and y-shifts and rotation), and the downstream triplet is aligned relatively to the upstream triplet (x, y- and z-shifts). While for the telescope alignment the coordinates of the hits are changed (active transformations), for the DUT the coordinates of the reference frame are changed instead (passive transformations) and all corrections are applied only to the track. The intersection of the telescope tracks with the tilted DUT is calculated and transformed into DUT coordinates to allow detailed DUT studies.

2S module alignment

The alignment of the DUT itself is primarily based on profile plots and projections and for its implementation it is assumed that the 2S sensors are planar. The alignment consists of a set of shifts of axes, rotations around the beam axis and adjustments of the tilt angle and the skew angle. The method converges after a few iterations.

Tracks inclined along the strips (EUTelescope)

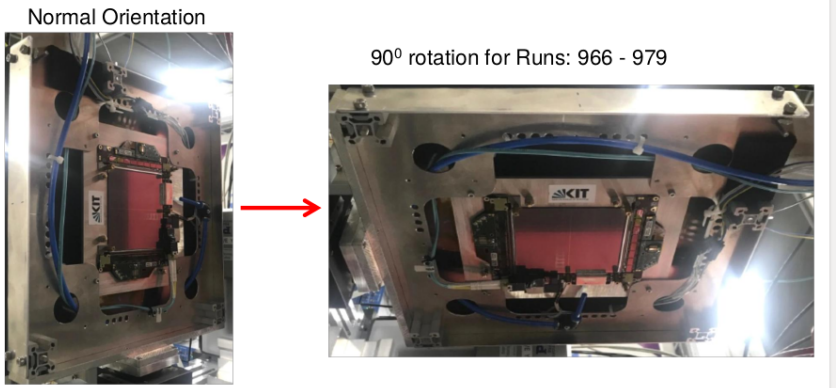

Before, the length of the strips was along the y-axis (vertical axis), here it was along the x-axis (horizontal axis)
Steady $x = 114.662\,\text{mm}$ and $y = 47.278\,\text{mm}$ and rotations about the y-axis